Argonne NATIONAL LABORATORY

ANL-GenIV-075

Status of Reactor Physics Activities on Cross Section Generation and Functionalization for the Prismatic Very High Temperature Reactor, and Development of Spatially-Heterogeneous Codes

Nuclear Engineering Division

About Argonne National Laboratory

Argonne is a U.S. Department of Energy laboratory managed by The University of Chicago under contract W-31-109-Eng-38. The Laboratory's main facility is outside Chicago, at 9700 South Cass Avenue, Argonne, Illinois 60439. For information about Argonne, see www.anl.gov.

Availability of This Report

This report is available, at no cost, at http://www.osti.gov/bridge. It is also available on paper to the U.S. Department of Energy and its contractors, for a processing fee, from:

U.S. Department of Energy
Office of Scientific and Technical Information
P.O. Box 62
Oak Ridge, TN 37831-0062
phone (865) 576-8401
fax (865) 576-5728
reports@adonis.osti.gov

Disclaimer

This report was prepared as an account of work sponsored by an agency of the United States Government. Neither the United States Government nor any agency thereof, nor The University of Chicago, nor any of their employees or officers, makes any warranty, express or implied, or assumes any legal liability or responsibility for the accuracy, completeness, or usefulness of any information, apparatus, product, or process disclosed, or represents that its use would not infringe privately owned rights. Reference herein to any specific commercial product, process, or service by trade name, trademark, manufacturer, or otherwise, does not necessarily constitute or imply its endorsement, recommendation, or favoring by the United States Government or any agency thereof. The views and opinions of document authors expressed herein do not necessarily state or reflect those of the United States Government or any agency thereof, Argonne National Laboratory, or The University of Chicago.

ANL-GenIV-075

Status of Reactor Physics Activities on Cross Section Generation and Functionalization for the Prismatic Very High Temperature Reactor, and Development of Spatially-Heterogeneous Codes

by
C.H. Lee, Z. Zhong, T.A. Taiwo, W.S. Yang, M.A. Smith, and G. Palmiotti
Nuclear Engineering Division, Argonne National Laboratory

August 31, 2006

TABLE OF CONTENTS

Page

TABLE OF CONTENTS 3

LIST OF FIGURES 5

ABSTRACT 7

1.0 INTRODUCTION 9

2.0 CROSS SECTION GENERATION AND FUNCTIONALIZATION 13

2.1 Description of VHTR Core and Components 13

2.2 Cross Section Representation 17

2.3 Fuel Block Cross Sections 28

2.4 Reflector Cross Sections 30

2.5 Control Rod Cross Sections 34

2.6 Energy Group Study 43

2.7 Pin Power Factors 46

3.0 X-MANAGER 48

4.0 SPATIALLY-HETEROGENEOUS CODE DEVELOPMENT 52

4.1 DeCART Code Development at KAERI (ROK) 53

4.2 UNIC Code Development 57

4.3 Final Comments 60

5.0 CONCLUSIONS 61

REFERENCES 64

LIST OF TABLES

Page

Table 1. VHTR Fuel Element Data. 15

Table 2. Number Densities of Burnable Poison and Control Rod Materials. 16

Table 3. Comparisons of Fuel Element Multiplication Factor at 300 K. 17

Table 4. Multiplication Factors at 99 GWd/t Burnup. 20

Table 5. k-infinity Error Due to Cross Section Interpolation Error. 21

Table 6. k-infinity Estimation Error from Cross Section Functionalization Scheme at Zero Burnup. 26

Table 7. Comparison of DRAGON and DIF3D Multiplication Factors for 1-D Fuel-Reflector Model without Control Rod. 32

Table 8. Comparison of DRAGON and DIF3D Multiplication Factors for 1-D Fuel-Reflector Model with Control Rod. 34

Table 9. Control Rod Worths of 7-Block Cores from MCNP and DRAGON/DIF3D 37

Table 10. Multiplication Factor and Rod Worth of Seven-Block Model (Type A). 40

Table 11. Comparison of MCNP and DRAGON Multiplication Factors for Rodded Fuel Block. 42

Table 12. Choice of Energy Group Boundaries. 44

Table 13. DRAGON and DIF3D Multiplication Factors for Energy Group Study. 45

Table 14. Comparison of Control Rod Worths with Different Number of Energy Groups. 45

Table 15. Comparison of DeCART and MCNP and HELIOS Results for VHTR Assembly. ... 56

LIST OF FIGURES

Page

Figure 1. Link between DRAGON and REBUS-3/DIF3D Codes. 11

Figure 2. VHTR Core Radial Arrangement. 14

Figure 3. Standard Fuel Block of VHTR. 15

Figure 4. Control Rod Configurations in Fuel and Reflector Regions. 16

Figure 5. Structure of ISOTAB File. 19

Figure 6. Differences in Actinide Number Densities at 99 GWd/t. 20

Figure 7. Burnup Dependence of Absorption Cross Sections. 23

Figure 8. Temperature Dependence of U-235 and U-238 Absorption Cross Sections. 24

Figure 9. Temperature Dependence of Graphite Up-scattering Cross Section of Graphite. 24

Figure 10. Comparison of k-infinity between DRAGON and DIF3D with Fitted Cross Sections at 0 Burnup. 25

Figure 11. Fuel Block Model for DF Calculation in DRAGON. 29

Figure 12. Comparison of 23-Group DFs for Fuel Blocks With and Without BP. 30

Figure 13. Two-Dimensional Core Slice Model. 31

Figure 14. Simplified One-Dimensional Slab Fuel-Reflector Model. 31

Figure 15. Comparison of Surface Fluxes at Interface between Fuel and Reflector. 33

Figure 16. One-Dimensional Slab Geometry Model for Control Rod. 34

Figure 17. Comparison of Surface-Average Fluxes at Interface between Fuel and Rodded Reflector with and without DFs. 35

Figure 18. Two-Dimensional Modeling for the Rodded Reflector Region. 36

Figure 19. Generation of Control Rod Cross Sections (Option A). 37

Figure 20. Generation of Control Rod Cross Sections (Option B). 38

Figure 21. 23-Group Surface-Dependent Discontinuity Factors of Seven-Block Rodded Models. 39

Figure 22. Power Comparison between MCNP and DRAGON/DIF3D for 2-D Seven-Block Model. 40

Figure 23. Geometry Approximation of Rodded Fuel Block Model. 41

Figure 24. Pin Indexing for Hexagonal Geometry. 46

Figure 25. Process for Generating Pin Power File in DRAGON. 47
Figure 26. Pin Power Distribution Determined from DRAGON Calculation. 47
Figure 27. Data Flow for DRAGON, X-MANAGER, and REBUS-3/DIF3D. 49
Figure 28. Functions and Libraries of X-MANAGER. 50
Figure 29. Structural Units of Hexagonal Assembly. 55
Figure 30. VHTR Fuel Block with Control Rod Hole. 57
Figure 31. CUBIT Rendition of a Prismatic VHTR Fuel Block (Meshing indicated). 60

ABSTRACT

The cross section generation methodology and procedure for design and analysis of the prismatic Very High Temperature Gas-cooled Reactor (VHTR) core have been addressed for the DRAGON and REBUS-3/DIF3D code suite. Approaches for tabulation and functionalization of cross sections have been investigated and implemented. The cross sections are provided at different burnup and fuel and moderator temperature states. In the tabulation approach, the multigroup cross sections are tabulated as a function of the state variables so that a cross section file is able to cover the range of core operating conditions. Cross sections for points between tabulated data points are fitted simply by linear interpolation. For the functionalization approach, an investigation of the applicability of quadratic polynomials and linear coupling for fuel and moderator temperature changes has been conducted, based on the observation that cross sections are monotonically changing with fuel or moderator temperatures. Preliminary results show that the functionalization makes it possible to cover a wide range of operating temperature conditions with only six sets of data per burnup, while maintaining a good accuracy and significantly reducing the size of the cross section file. In these approaches, the number of fission products has been minimized to a few nuclides (I/Xe/Pm/Sm and a lumped fission product) to reduce the overall computation time without sacrificing solution accuracy.

Discontinuity factors (DFs) based on nodal equivalence theory have been introduced to accurately represent the significant change in neutron spectrum at the interface of the fuel and reflector regions as well as between different fuel blocks (e.g., fuel elements with burnable poisons or control rods). Using the DRAGON code, procedures have been established for generating cross sections for fuel and reflector blocks with and without control absorbers. The preliminary results indicate that the solution accuracy is improved by using the discontinuity factors along with the nodal cross sections.

In order to efficiently manage the cross section generation procedures, the X-MANAGER toolkit has been developed, with its functions programmed with UNIX shell commands. The toolkit helps to (1) submit multiple DRAGON jobs for different temperature conditions, (2) merge many ISOTXS files into one ISOTAB file, (3) generate reflector cross sections by executing DRAGON and an auxiliary finite difference code for the 1-D fuel-reflector model, (4) create

delta-macroscopic cross sections for control rods comparing un-rodded and rodded ISOTAB files, and so on. In the future, the X-MANAGER toolkit will be extended with more functions for an advanced level of automation.

The parallel development of spatially heterogeneous codes is being pursued under other USDOE and international programs. The status of two of these codes (UNIC and DeCART), being leveraged by this project, was reviewed in this work. It was found that much effort is required before these codes can be used for routine evaluations of the prismatic VHTR design.

1.0 INTRODUCTION

The prismatic Very High Temperature Reactor (VHTR) is one of the leading candidates for the Next Generation Nuclear Plant (NGNP) in the U.S. [1, 2] In this design, fuel rods (compacts) are contained in fuel holes in the hexagonal-prismatic fuel elements. Fuel elements also have holes for coolant and control rod material passages, and fuel element handling. The cylindrical fuel compacts contain coated fuel particles (CFPs) dispersed in a graphite matrix. The CFPs give an additional level of heterogeneity within the fuel element.

For design and analysis of the VHTR cores, computational codes are required to have adequate physics models that are able to represent the core characteristics. The double heterogeneity of VHTR fuel elements caused by the use of the coated fuel particles is one of the most distinct characteristics that have to be properly treated in neutronics analysis. The choice of an annular core makes neutron leakage into the inner and outer reflectors more important than in traditional light water reactors (LWRs) because high power peaks can occur at the core-reflector interfaces. Accurate predictions of the core reactivity, flux and power distributions, and depletion characteristics are crucial in designing economical and safe reactors. Also, for routine design analyses, which require thousands of repeated calculations, efficient computational tools are required.

Computational tools that are available for use in the neutronic design and analysis of the VHTR have been reviewed in a previous study. [3, 4] For lattice physics calculations, DRAGON [5] or WIMS8 [6] was found to be adequate, allowing the detailed treatment of the double heterogeneity effect of coated fuel particles of the VHTR design at the assembly level and providing accurate representation of single-assembly power distributions and multiplication factors. Since WIMS8 is a proprietary code, DRAGON was considered as a primary candidate for physics calculations even though further validation and verification would be required because of its limited use for advanced gas-cooled reactor design. For whole-core calculations, REBUS-3/DIF3D [7, 8] developed at Argonne was selected as the calculation code suite, with a plan to implement the required functionalities for prismatic block-type VHTR applications.

The DRAGON code has a collection of models for simulating the neutronics behavior of a unit cell or a fuel assembly in a nuclear reactor. The typical functionalities found in most modern lattice codes are contained in DRAGON. These include interpolation of microscopic cross sections supplied by means of standard libraries, resonance self-shielding calculations in multidimensional geometries, multigroup and multidimensional neutron flux calculations, and modules for editing condensed and homogenized nuclear properties for reactor calculations. The code also performs isotopic depletion calculations. Macroscopic cross sections can also be read via the input data stream. In the present study, the 69- and 172-group cross section libraries created in WIMSD4-format by the Reduced Enrichment for Research and Test Reactors (RERTR) project are used.

In the preliminary assessment [3], the accuracy of the DRAGON code for VHTR fuel element analyses was evaluated by comparing its solutions with those from the high fidelity MCNP4C code [9], using ENDF/B-VI nuclear data. In this work, the accuracy evaluation is extended for reflector blocks and fuel blocks with burnable poisons or control rods.

The DIF3D and REBUS-3 codes are used for whole-core flux calculations and fuel cycle analyses. The DIF3D core solves the three-dimensional multigroup diffusion or transport equations for given core configurations. It has several solution options such as the finite difference diffusion theory method (FDM), the nodal expansion diffusion theory method based on the transverse integration procedure, and the VARIANT nodal transport method. [10] The current VARIANT option allows high-order spatial and angular approximations (up to sixth-order non-separable polynomial approximation in space and P_5 approximation in angle). The REBUS-3 code performs depletion calculations using the neutron fluxes provided by DIF3D and provides new composition data for DIF3D. It also performs the fuel shuffling and reloading operations.

Since the REBUS-3/DIF3D system was originally developed for fast reactor analyses it has a limited capability to represent the burnup dependency of cross sections. The cross sections of VHTR fuel elements vary significantly with burnup and fuel and moderator temperatures. Thus, a more general capability to represent the cross sections as a function of burnup and

temperatures needs to be implemented. The newly developed cross section representation schemes are discussed in Section 2.0.

To accurately model prismatic VHTR cores, the cross sections of individual components (fuel block, reflector, control rod, burnable poisons, etc.) should be adequately generated in lattice physics calculations. Especially, the large local power changes near the core-reflector interface require accurate reflector cross sections to preserve the reaction rates of reflector and the leakages at the interface. It is also challenging to generate the cross sections of a reflector block with a control rod inserted because of significant heterogeneity effects. In addition, since a control rod is loaded asymmetrically in reflector or fuel elements, surface-dependent leakage effects should be considered for accurate estimation of power distribution. An accurate and practical cross section representation model for VHTR cores was developed in this study and necessary verification tests of the proposed models were carried out through benchmark calculations. These issues are also discussed in Section 2.0.

To generate the multigroup cross sections of all the core elements for all operating conditions, a large number of DRAGON jobs need to be run and significant data manipulations are necessary. For a user-friendly data management, a toolkit named X-MANAGER (Cross-Section Manager) has been developed, which contains many functions to automate routine jobs. As shown in Figure 1, the cross sections generated from DRAGON are adjusted using the nodal equivalence parameters and merged into a single dataset for REBUS-3/DIF3D calculations. The X-MANAGER capabilities are presented in Section 3.0.

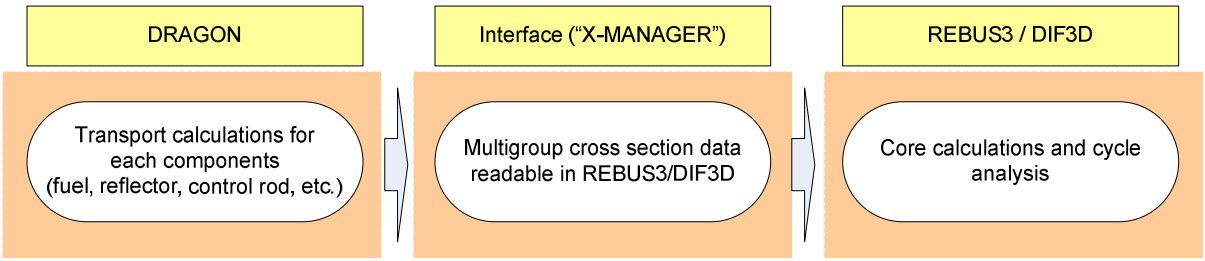

Figure 1. Link between DRAGON and REBUS-3/DIF3D Codes.

In Section 4.0, a review of the current status of the spatially heterogeneous code capabilities that are being developed under other USDOE and international programs is provided. These efforts are being leveraged by this VHTR/NGNP project to ensure that they provide a tool that could be used for analysis of advanced nuclear reactor designs, including the prismatic VHTR type.

Conclusions from this work are presented in Section 5, along with descriptions of the pending tasks that are needed for the prismatic VHTR code suite.

2.0 CROSS SECTION GENERATION AND FUNCTIONALIZATION

2.1 Description of VHTR Core and Components

The general specifications of the core and its elements are summarized in this section. The data will be used for the verification tests of the cross section generation methods proposed in the following sections. The VHTR core defined in this report is based on the NGNP reactor design [2] which consists of hexagonal graphite fuel and reflector elements, and reactivity control materials. The core is designed for a power level of 600 MWt and a power density of 6.6 W/cm^3. The whole core is composed of 11-ring hexagonal columns, in which the active core has 102 fuel columns that are located in rings 6, 7, and 8. Ten graphite fuel elements (blocks) stacked vertically comprise a fuel column. The height of the active core is 793 cm and the effective inner and outer diameters are 296 cm and 483 cm, respectively. Each fuel element contains holes for fuel and burnable compacts, and full-length channels for helium coolant flow. The inner five rings of the core contain removable graphite columns. Removable columns are also located in rings 9 and 10. Beyond the outer removable columns are the permanent side reflectors.

The core reactivity is controlled by a combination of lumped burnable poison and movable control rod. In the event that the movable control rods are inoperable, an independent reserve shutdown control is utilized. This control mechanism employs borated pellets that are released into the reserve shutdown channel in the active core.

The principal fuel element structural material is H-451 graphite (density is 1.74 g/cm^3) in the form of a right hexagonal prism, with a flat-to-flat width of 36 cm. There are three different types of fuel elements: standard fuel element, reserve shutdown element, and control element. The standard fuel element contains fuel and coolant holes arranged in a triangular lattice and a central handling hole. The ratio of fuel holes to coolant holes is about 2. The control and reserve shutdown elements differ from the standard fuel elements in that they contain a large diameter hole for control rods/materials. This hole replaces 24 fuel and 11 coolant holes and its diameter is 9.53 cm in the reserve shutdown element and 10.16 cm in the control element.

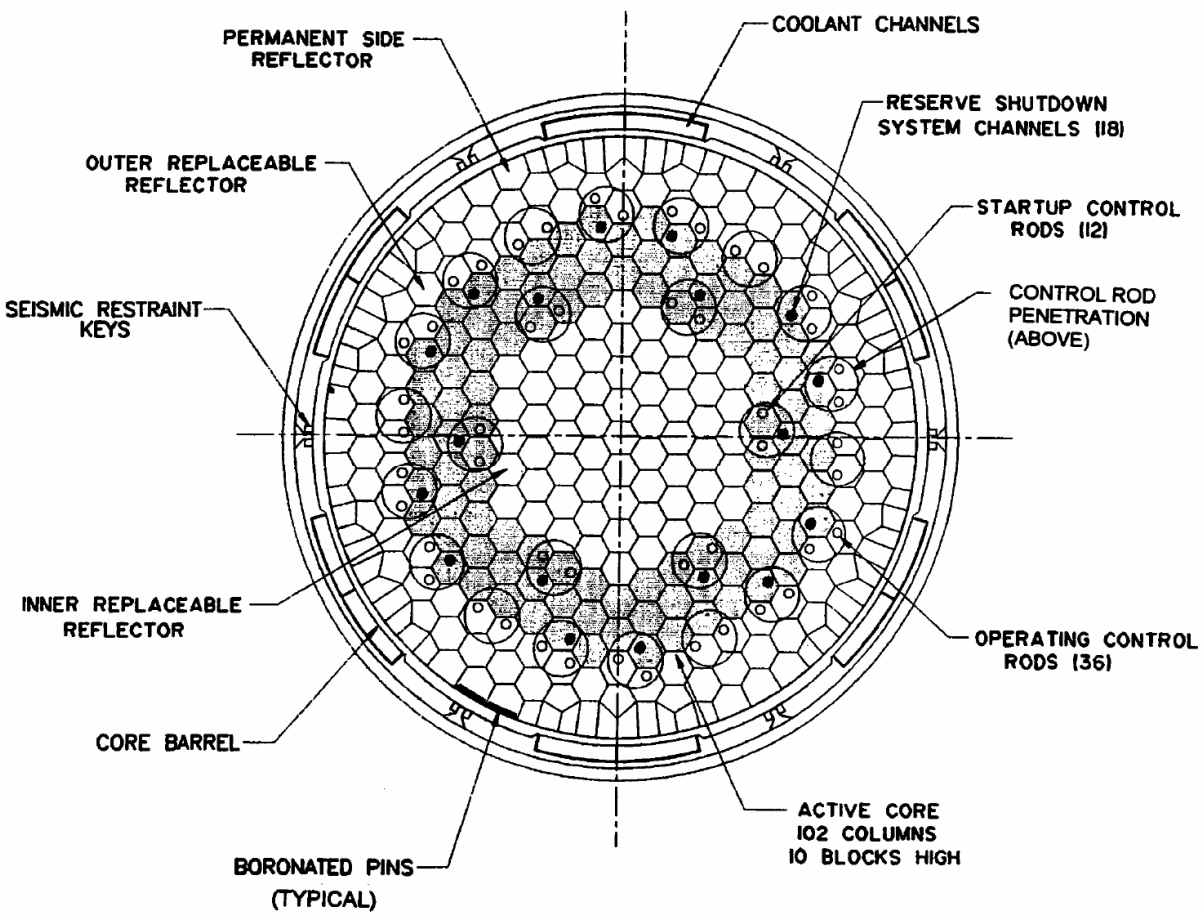

Figure 2. VHTR Core Radial Arrangement.

Each fuel compact has a diameter of 1.245 cm and a height of 4.93 cm. Coated fuel particles (TRISO) are dispersed in the compact graphite medium. In the current conceptualization of the VHTR, only fissile fuel is being considered for non-proliferation reasons. The fuel form is uranium oxy-carbide ($UC_{0.5}O_{1.5}$), which prevents CO gas formation and thus minimizes kernel migration of UO_2. Table 1 presents the fuel compact data. The fuel element has 216 fuel holes (including six lumped burnable poison holes) and 108 coolant holes (see Figure 3). The poison rods consist of B_4C granules dispersed in graphite compacts. The pitch of the coolant hole or fuel compact is 1.8796 cm and the radii of the fuel compact and fuel holes are 0.6223 and 0.635 cm, respectively. There are 102 large coolant holes with 0.794 cm radius and 6 small coolant holes with 0.635 cm radius.

Table 1. VHTR Fuel Element Data.

	Radius, cm	Material	Density, g/cc
Fuel Particle - Fuel kernel - Buffer - Inner Pyro-Carbon - SiC - Outer Pyro-Carbon	 0.0175 0.0275 0.0310 0.0345 0.0385	 $UC_{0.5}O_{1.5}$ Graphite Graphite SiC Graphite	 10.50 1.00 1.90 3.20 1.87
Fuel compact	0.6225	Graphite	1.1995
Coolant	0.6350	He	0.0032
Graphite Element		Graphite	1.74

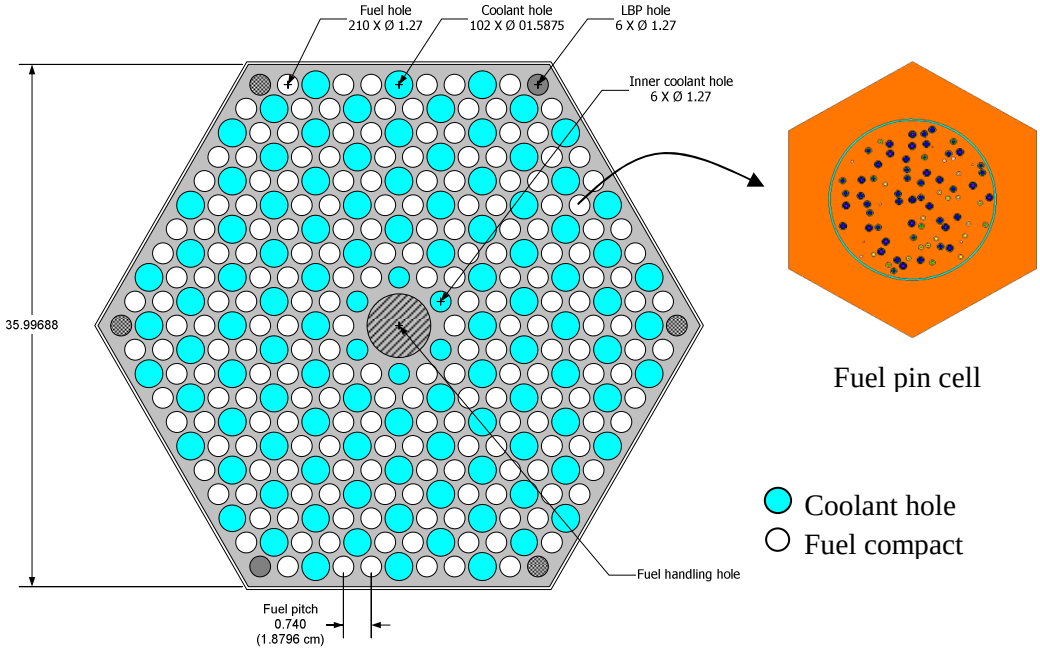

Figure 3. Standard Fuel Block of VHTR.

Thirty-six of the outer reflector columns and twelve core columns have channels for control rods. While the twelve in-core columns are reserved for start-up and shutdown functions, the thirty-six control rods located in the outer reflector are used for operational power control and

reactor trip. Additionally to these rods, there are 18 columns in the active core containing channels for reserve shutdown material. A control rod is located in one 1/6-sector of fuel and reflector blocks, as shown in Figure 4. The control rod material consists of 40 w/o enriched boron (90% B-10), contained in B_4C granules dispersed uniformly in a graphite matrix and formed into annular compacts. The reserve shutdown control material consists of 40 w/o natural boron in B_4C granules dispersed uniformly in a graphite matrix and formed into pellets. The B_4C granules are coated with dense pyrolytic carbon (PyC) to minimize oxidation and boron loss during high temperature, high moisture off-normal events. In this study, homogenized burnable poison and control rod were used for simplicity, with the number densities listed in Table 2.

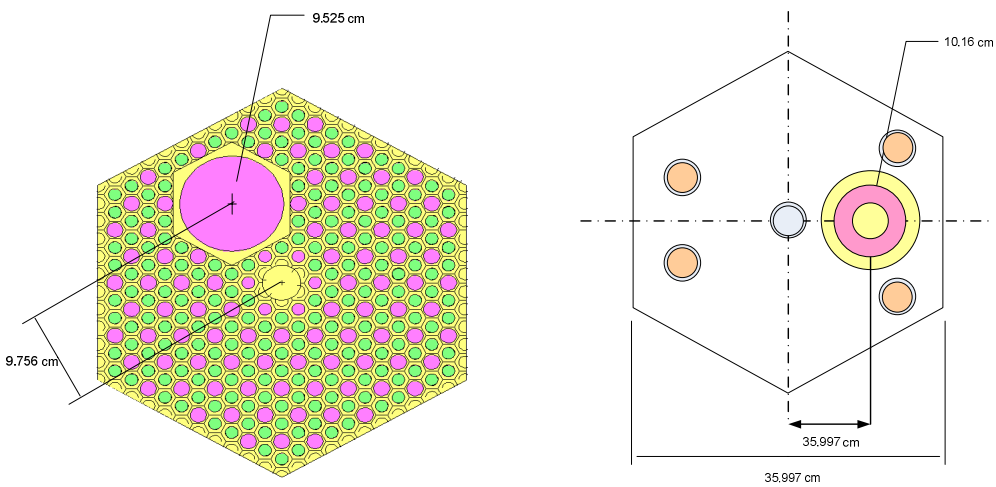

(Fuel Region) (Reflector Region)

Figure 4. Control Rod Configurations in Fuel and Reflector Regions.

Table 2. Number Densities of Burnable Poison and Control Rod Materials.

Element	Material	Number Density (#/cm^3)
BP rod	B-10 B-11 Graphite	1.58597E-04 1.60337E-05 6.24123E-02
Control Rod	B-10 B-11 Graphite	1.05773E-02 1.06891E-03 1.47097E-02

The DRAGON code has been run for the VHTR fuel element at 300 K, and its results compared with those from the high fidelity MCNP4C code. Both MCNP4C and DRAGON used cross section libraries based on ENDF/B-VI nuclear data. Table 3 indicates that both MCNP4C and DRAGON results agree well when the homogeneous fuel compact model is used, and the double heterogeneity effect is overestimated in DRAGON by about 0.5 %Δρ. In order to isolate the errors associated with the cross section tabulation and functionalization, the homogeneous fuel compact model is used for testing the cross section generation methods to be discussed in the following sections. However, heterogeneous fuel compacts with explicit TRISO particle representation are also used in the verification calculations.

Table 3. Comparisons of Fuel Element Multiplication Factor at 300 K.

Configuration	Fuel Block	MCNP4C	DRAGON	%Δρ
Homogeneous Fuel Compact	w/o BP	1.47433 (±0.00027)	1.47522	0.041
	w/ BP	1.20780 (±0.00031)	1.20982	0.138
Explicit TRISO Particles	w/o BP	1.52908 (±0.00030)	1.54061	0.490
	w/ BP	1.25252 (±0.00022)	1.26129	0.555

2.2 Cross Section Representation

The current version of REBUS-3/DIF3D, originally developed for fast reactors, reads an ISOTXS file for cross section data and performs fuel cycle analysis as well as depletion calculations. It has only a limited capability to treat the burnup dependency of cross sections, since in fast reactors cross sections do not vary strongly with fuel burnup or temperature changes. In thermal reactors, however, cross sections change significantly with burnup and temperature changes. In addition, the local flux changes at the interfaces of different fuel elements are more pronounced. To estimate core fluxes, powers, and reactivities accurately, the cross sections for core calculations need to be represented as a function of state parameters such as burnup, fuel and moderator temperatures, etc.

The cross section representation scheme is required to (1) cover the possible operating range of burnup, and moderator and fuel temperatures in the VHTR core, (2) represent all components of the core with sufficient accuracy, and (3) use a flexible number of energy groups,

limited by memory and storage sizes. In principle, more parameters such as fuel enrichment and packing fraction, etc., can be added to the cross section representation, but only three major parameters, burnup, and fuel and moderator temperatures, have been taken into account in this work.

The tabulation with parameters is the simplest and most stable form of cross section representation, but it requires relatively large amount of data points to maintain the required accuracy. The functionalization with parameters is normally more efficient than the tabulation, but it requires an effort to find appropriate functional forms and may result in a loss of accuracy in estimating data, even within the parameter range of interest. It was decided to use the tabulation method for cross section representation, but the functionalization approach was also investigated for future use.

Cross Section Tabulation

Although the tabulation approach requires a relatively large data storage space, it is a very simple and stable form of organizing data for a large number of state parameters involved. In the current VHTR design, the coolant temperature rise across the core is about 500 K and the temperature difference between coolant and moderator or between moderator and fuel is less than 200 K at normal operating conditions. A 100 K interval for moderator temperature was found to be adequate for tabulation of cross sections. For this temperature interval, the optimized number of total data points might not be overwhelming.

For a fuel element design, the DRAGON code generates the cross sections at various conditions in ISOTXS format. A large number of ISOTXS files corresponding to different states (burnup and temperature) are generated, and they are merged into a single file named ISOTAB for REBUS-3/DIF3D calculations. In this merging step, the cross section data are re-organized as shown in Figure 5; the cross sections are systematically sorted with state parameters. Similar to the ISOTXS file, the cross section data is categorized by isotopes in ISOTAB. The cross sections of an isotope is tabulated in a nested loop; first with respect to the burnup state and then with respect to the fuel and moderator temperatures. If a new state parameter is introduced, then another loop would be placed inside the burnup loop.

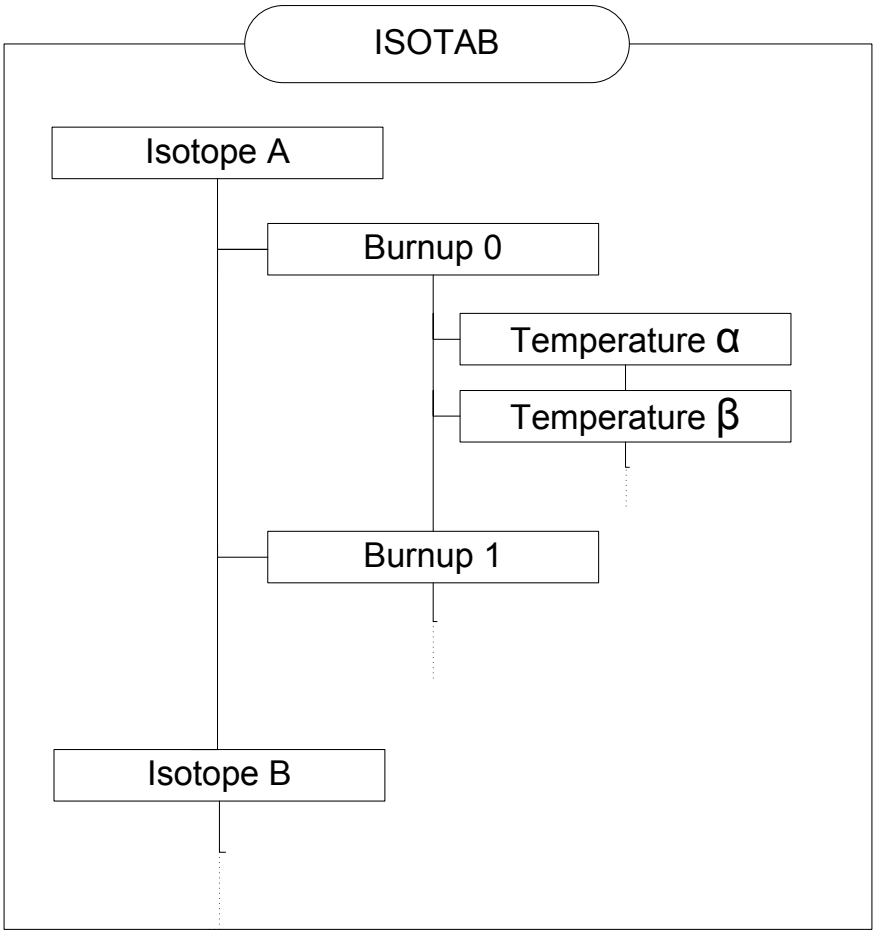

Figure 5. Structure of ISOTAB File.

History Effect of Cross Sections

If a fuel block irradiated at different temperatures is evolved to significantly different isotopic compositions at the same burnup after long depletion, the operating temperature history needs to be included in the cross section representation. This would make the cross section representation scheme more complicated. In order to assess the operating temperature history effect, depletion calculations were performed with the DRAGON code for two fuel temperatures, 1043 K and 1243 K, up to a burnup of 99 GWd/t. To separate the temperature history effect from the instantaneous temperature effect, the nuclide densities at several burnup states were extracted from the depletion calculation results for 1043 K, and static calculations were performed at 1243 K. Figure 6 shows the nuclide density differences of major isotopes and Table 4 compares the multiplication factors at 99 GWd/t burnup.

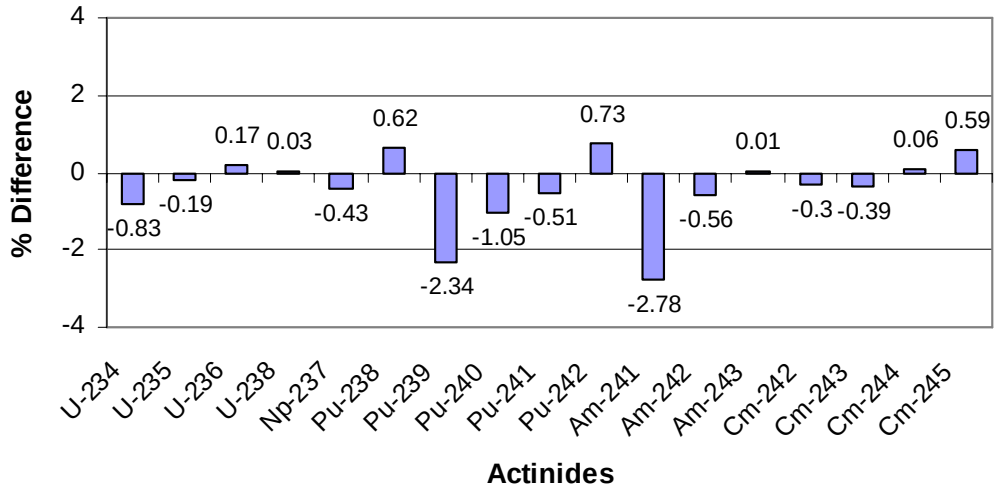

(% difference = ($k_{\infty}^{1043K} / k_{\infty}^{1243K}$ - 1) x 100)

Figure 6. Differences in Actinide Number Densities at 99 GWd/t.

As can be seen in Figure 6, different fuel depletion temperatures cause only marginal differences in the isotopic densities even at a high burnup of 99 GWd/t. The difference in k-infinity between the two depletion cases is 418 pcm. This difference is the combined effect of different isotopic densities and fuel temperatures. From the results in Table 4, it can be deduced that most of this difference is due to the difference in fuel temperature and the effect of different nuclide densities is only 40 pcm Δk. In other words, the temperature history effect is much smaller than the instantaneous temperature effect. This indicates that in the thermal feedback calculation, cross sections can be determined with the current temperatures without introducing a significant error.

Table 4. Multiplication Factors at 99 GWd/t Burnup.

Calculation Scenario	k-infinity (Δk)
Depletion with 1043 K (A)	1.10739
Depletion with 1243 K (B)	1.10321
Depletion with 1043 K up to 99 GWd/t and then temperature change to 1243K (C)	1.10281
Δk, (A – B)	(418 pcm)
Δk, (B – C)	(40 pcm)

Interpolation of Cross Section Tables

A fully tabulated approach with a piecewise linear interpolation scheme was initially employed for cross section evaluation at given state conditions. A preliminary study showed that the piecewise linear interpolation results in non-negligible interpolation errors if the temperature grid size is greater than 100 K. This requires a huge data size (several hundred megabytes, possibly gigabytes) to cover the large temperature range of the prismatic VHTR with a relatively fine temperature interval. In order to reduce the data size, a quadratic interpolation scheme for fuel and moderator temperature effects was investigated. In this scheme, the cross section variation is represented by a quadratic polynomial of the variations of the moderator temperature and the square root of fuel temperature, using surrounding nine data points.

To test this quadratic interpolation scheme, the microscopic cross sections at nine temperature points (moderator temperatures of 773 K, 973 K, and 1173 K and fuel temperatures of 843 K, 1043 K, and 1243 K) were generated using the DRAGON code. Using these data, the cross sections at the moderator temperature of 1073 K and the fuel temperature of 1143 K were interpolated for various burnup states by linear and quadratic schemes, and then DIF3D calculations were performed using these interpolated cross sections. To isolate the cross section interpolation error, the reference isotope densities obtained from the DRAGON calculation were used in DIF3D calculations. The resulting k-infinity values are compared with the DRAGON results in Table 5.

Table 5. k-infinity Error Due to Cross Section Interpolation Error.

Burnup (GWd/t)	Reference DRAGON k-inf	DIF3D, Δk (pcm)	
		Linear Interpolation	Quadratic Interpolation
0	1.55258	92	36
0.036	1.53420	91	38
0.146	1.49755	86	38
0.510	1.48370	84	36
4.370	1.45035	99	39
48.10	1.27924	120	21
99.20	1.10384	272	56
150.0	0.87724	218	48
191.0	0.67146	288	73

It is noted that the k-infinity error due to the cross section interpolation error generally increases with burnup because of the temperature history effects. As can be seen, the quadratic interpolation scheme is superior to the linear interpolation. This result indicates that the quadratic interpolation scheme would allow the use of a coarser temperature grid. However, it was found that the second-order interpolation scheme does not reduce the number of data points significantly and makes its application in a whole-core calculation more complicated, thus it was decided to use the linear interpolation for the actual implementation.

Study of Cross Section Functionalization

As aforementioned, the fully tabulated dataset for multiple independent variables requires a large storage space. It is expected to exceed several hundred megabytes, possibly gigabytes when there are many different components or fuel types in the core. In order to investigate a potential way to reduce the dataset size without sacrificing the representation accuracy, the functional relations of microscopic cross sections to burnup, moderator and fuel temperature were examined. Using the DRAGON lattice code, homogenized cross sections were generated for a VHTR fuel block with fuel enrichment of 14%, fuel particle packing fraction of 0.25, and fuel kernel radius of 215 μm. Since the cross section variations become more pronounced with decreasing number of energy group, a four-energy group structure (with upper energy boundaries of 10 MeV, 1.353 MeV, 9.118 keV, and 0.4 eV) was used. A larger number of energy groups are expected to be required for VHTR analyses (especially with increasing amount of transuranic elements), but the cross section functionalization would be easier for a larger number of groups because the cross section variations become less pronounced.

Figure 7 shows the burnup dependence of microscopic absorption cross sections in the aforementioned four-group structure. Relative value to the average value over the burnup range of interest is shown for the microscopic cross sections of U-235, U-238 and Pu-239. The burnup dependence of the absorption cross section is rather smooth except for the Group-3 cross section of Pu-239 which shows a sharp decrease at very low burnup. At zero burnup where no Pu-239 is present, it is not self-shielded and thus a very large (infinite dilute) cross section results. As Pu-239 concentration increases with burnup, the self-shielding increases sharply and thus the cross section decreases accordingly. Other actinides not present in the fresh fuel (Pu-240,

Am-241, Cm-242, etc.) show similar trends. For these cross sections, the polynomial representation for burnup does not provide enough accuracy. Thus, it is proposed to use the fully tabulated approach for representing the burnup dependence.

Figure 8 shows the group-3 and group-4 absorption cross sections of U-238 and the group-4 absorption cross sections of U-235 as a function of the square root of fuel temperature at zero burnup and 1150 K moderator temperature. It can be seen that for a given moderator temperature, the cross section can be represented very accurately as a quadratic function of the square root of fuel temperature. It was also observed that the dependence of graphite cross sections on fuel temperature is negligible and their dependence on moderator temperature is also quadratic as shown in Figure 9 for up-scattering cross section.

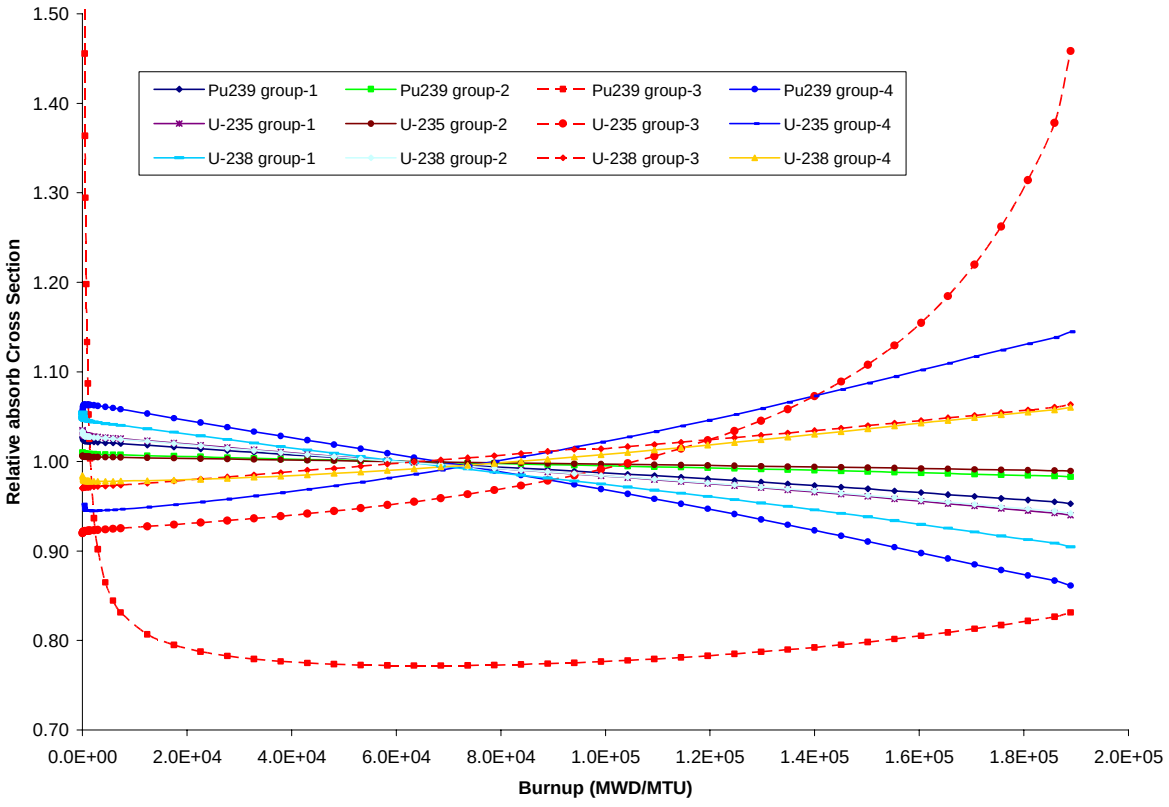

Figure 7. Burnup Dependence of Absorption Cross Sections.

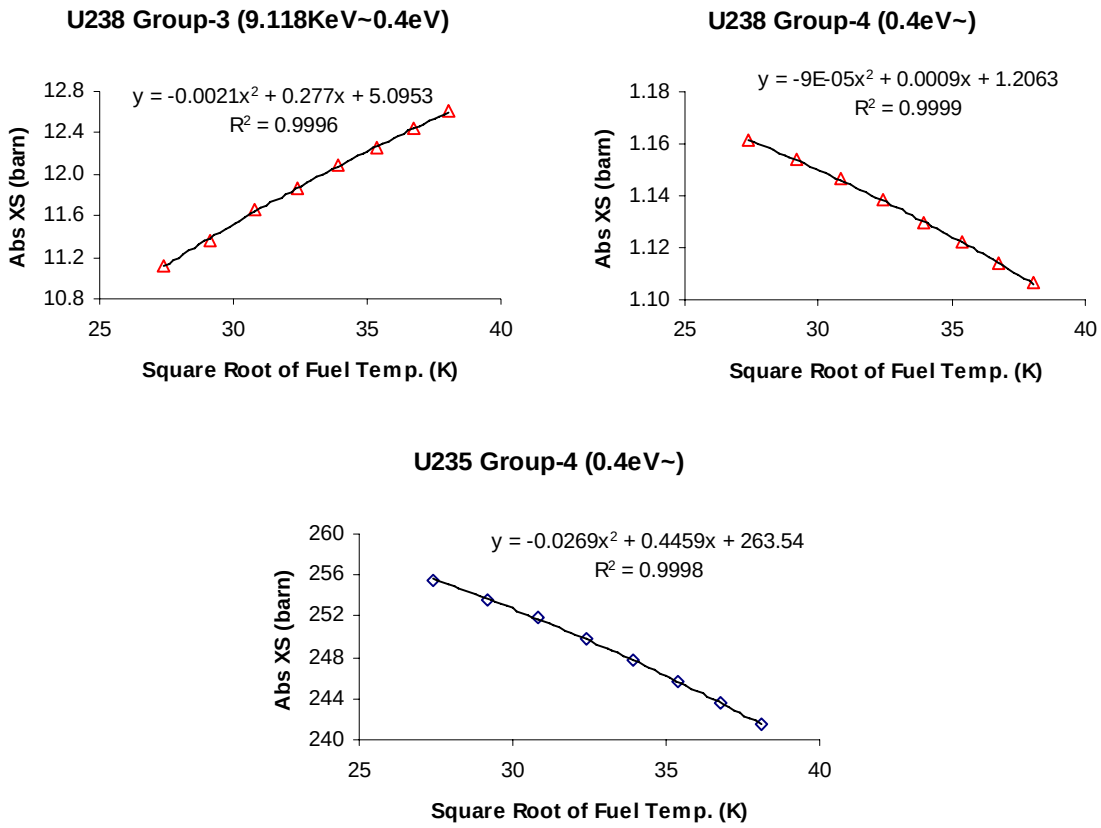

(Moderator Temperature: 1150 K)

Figure 8. Temperature Dependence of U-235 and U-238 Absorption Cross Sections.

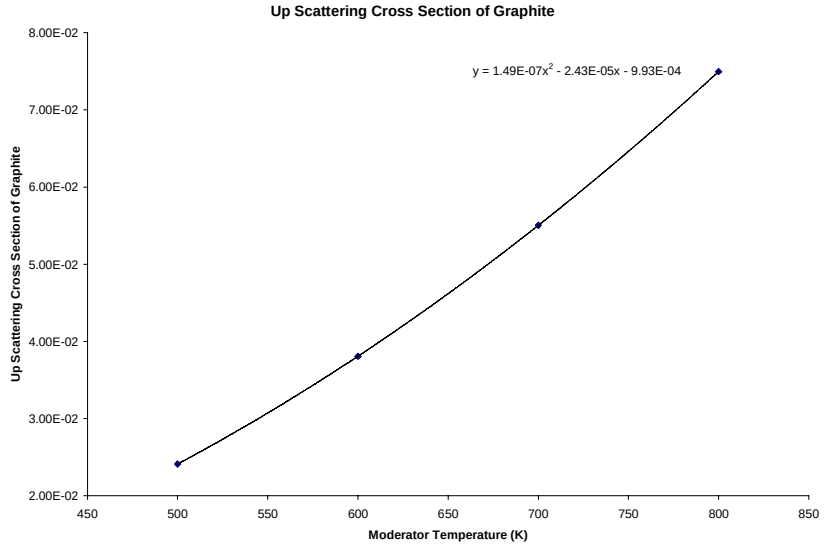

Figure 9. Temperature Dependence of Graphite Up-scattering Cross Section of Graphite.

Based on these observations, the following functional form is proposed to represent the dependences of cross sections on burnup (B), fuel temperature (T_f), and moderator temperature (T_m):

$$\begin{aligned}\sigma(B,T_m,\sqrt{T_f}) = \sigma(B,T_{m0},\sqrt{T_{f0}}) + a_1(B)\Delta T_m + a_2(B)\Delta T_m^2 \\ + b_1(B)\Delta\sqrt{T_f} + b_2(B)\Delta\sqrt{T_f}^2 + c(B)\Delta T_m \Delta\sqrt{T_f},\end{aligned} \tag{1}$$

where $\Delta T_m = T_m - T_{m0}$, $\Delta\sqrt{T_f} = \sqrt{T_f} - \sqrt{T_{f0}}$, T_{m0} = base moderator temperature, T_{f0} = base fuel temperature, B = burnup, and a, b, c = polynomial coefficients as a function of burnup. Base cross sections are calculated normally at average temperatures. Moderator and fuel temperature coefficients are calculated based on the Least Squares Method (LSM) with a sufficient number of data points that cover the whole temperature range of interest. Note that all the coefficients are simply a function of burnup.

The performance of this functionalization scheme was tested at zero burnup with 4- and 23-group cross sections of the VHTR fuel block. Fuel and moderator temperatures for base cross sections were set to 1150 K and 1100 K, respectively, and the coefficients a, b, and c were generated using LSM. In this test, the cross term of fuel and temperature variations was neglected by setting the coefficient c of Eq. (1) to 0. Figure 10 compares the multiplication factors of a fuel block determined from DIF3D calculations with fitted cross sections and the reference solutions obtained from DRAGON calculations. The results indicate that the fuel block cross sections can be accurately estimated with the proposed fitting function over a wide temperature range.

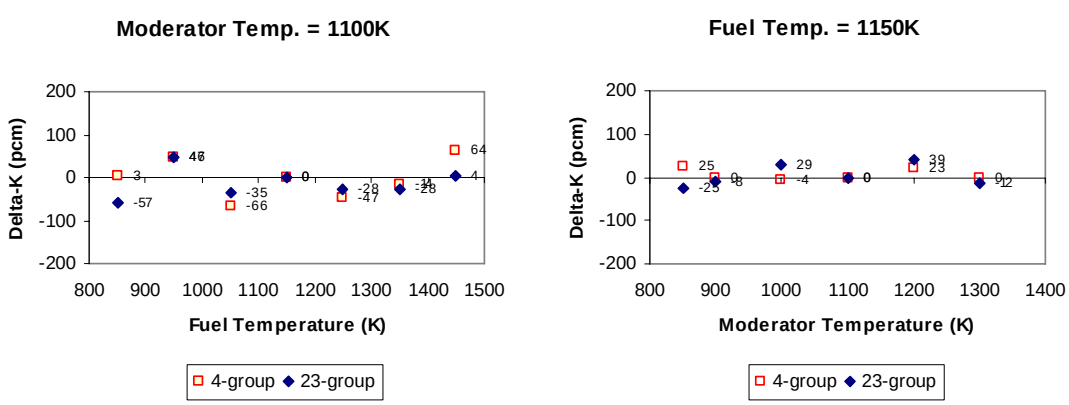

Figure 10. Comparison of k-infinity between DRAGON and DIF3D with Fitted Cross Sections at 0 Burnup.

Even when both fuel and moderator temperatures were changed from the base temperatures at the same time, the multiplication factors could be estimated within an acceptable range of error, as shown in Table 6. The new functionalization approach requires only six datasets per burnup to cover the entire operating temperature range, while the tabulation scheme needs many cross section datasets with a temperature interval of 100 K. However, further verification tests are required before implementing this functional scheme; more detailed examinations including the evolution of major nuclides with burnup need to be done, and other types of fuels (e.g., TRU fuel) need to be investigated.

Table 6. k-infinity Estimation Error from Cross Section Functionalization Scheme at Zero Burnup.

Fuel Temp (K)	Moderator Temp (K)	DRAGON k-inf	Δk (Fitting – DRAGON), pcm	
			4 group	23 group
1000	900	1.38223	-43	-8
1200	900	1.36566	-9	-45
1300	1000	1.35743	-20	-51
1300	1200	1.35561	-47	-28

Fission Product Modeling for Depletion

As aforementioned, the 69- or 172-group cross section libraries created in WIMSD4-format by the Reduced Enrichment for Research and Test Reactors (RERTR) project at Argonne are currently used for DRAGON calculations. To reproduce the isotope number densities of DRAGON in REBUS-3 calculations, the depletion chains in both codes should be consistent with each other. The cross section libraries used for DRAGON calculations have 38 fission products. Modeling of all these fission products in REBUS-3 whole-core depletion calculations requires a large cross section file and increases the required memory and computing time significantly. Thus, it was decided to employ a reduced set of fission products in the REBUS-3 calculations. The fission products, I-135, Xe-135, Pm-147, Pm-147m, Pm-148, Pm-148m, and Sm-149 are traced explicitly because they have relatively short half-lives and large absorption cross sections that change with core flux levels. The other fission products are merged and

treated as a single lumped fission product to save space, memory, and computing time. The number density of the lumped fission product (LFP) is made equivalent to the sum of the fission products merged and the cross sections are averaged with number densities. Detailed discussions are provided in Reference 11.

Generation of Equivalence Theory Based Discontinuity Factors

The nodal equivalence theory initially proposed by Koebke [12] and later generalized by Smith [13] has been found to be very effective for estimating the high-order heterogeneous solution by solving the corresponding low-order homogenous equation with additional parameters introduced to preserve the reaction rates, average fluxes, and average leakages of higher-order solution. The additional parameters called discontinuity factors (DFs) allow the homogeneous flux to be discontinuous between two adjacent homogenized regions.

Normally, fuel block cross sections are generated in the lattices physics calculations using a single assembly configuration with reflective boundary conditions, and DFs are calculated using the assembly-average and surface-average fluxes. The group constants and equivalence parameters determined from a single fuel block calculation would be adequate, provided the actual spectrum in the core is not significantly different from that of the single fuel block.

For reflector cross sections, a two-region problem composed of fuel and reflector blocks is used to perform the group condensation with more realistic neutron spectra. Discontinuity factors at the fuel-reflector interface are also calculated to preserve leakages through the interface. Similarly to the fuel block, as long as the neutron spectra of the two-region problem are close to the actual spectra in the core, these cross sections and DFs would provide a good accuracy.

In the generalized equivalence theory, a DF is defined for each nodal face so that the neutron current at each face is preserved. If the DFs of all the faces are identical or can be approximated by a single value due to the geometric symmetry, they can be incorporated directly into cross sections. This approximation is called the simplified equivalence theory, and the cross sections are adjusted as:

$$\sigma'_{\alpha g} = \sigma_{\alpha g} \times f_g \text{ , if } \alpha = \text{transport cross sections,} \quad (3)$$

$$\sigma'_{\alpha g} = \sigma_{\alpha g} / f_g \text{ , otherwise,}$$

where α = cross section type, g = group, and f_g = discontinuity factor for group g. Since in the VHTR cores the control rod is designed to be inserted at an asymmetric location in fuel or reflector blocks, the generalized equivalence theory is required to preserve the currents in all spatial directions. However, the current surface-dependent discontinuity factor capability of DIF3D is limited to the nodal *diffusion* theory option, which was found to be of insufficient accuracy for VHTR rodded configurations. For the moment, therefore, the simplified equivalence theory was employed, and the multigroup cross sections were adjusted with average discontinuity factors for the verification tests performed in the study. More details on generation of cross sections and DFs are provided in the following sections.

2.3 Fuel Block Cross Sections

Fuel block cross sections are generated based on single block calculations with reflective boundary conditions. Although the actual boundary conditions in the core are not the same as the single block conditions, this approximation would be adequate, provided the neutronic properties of neighboring nodes are similar to that of the node being considered.

The current version of DRAGON (Version 3.5) is able to model hexagonal cells containing circular pins, but it is not flexible enough to mix hexagonal and circular geometries in the assembly configuration. Thus, the fuel-element handling hole at a central position of the fuel block is approximated with 2-ring hexagonal cells (7 cells). Since the graphite density of the fuel-element handling hole is not different from that of normal fuel elements, this approximation would be valid.

It is noted that in the DRAGON full-assembly model for the VHTR hexagonal block, the block is formed by a collection of pin-cell sized hexagons. Each pin-cell contains the fuel compact surrounded by block graphite. When all the fuel and coolant-hole pin-cells are represented, the block graphite content is not totally accounted for and therefore an extra ring of pin-cell sized hexagons is used to represent the remaining graphite. The number density of the

graphite in these peripheral cells is modified to preserve the graphite content of the assembly block. Due to the use of the pin-cell sized hexagons, the DRAGON assembly model has jagged boundaries, and not the flat boundaries of the hexagonal block. Due to this jagged boundary model, it is not possible to directly calculate surface average fluxes for the generation of discontinuity factors. Although the modification of DRAGON for a flat boundary is an ultimate solution to the problem, small circular regions are temporarily added to the peripheral hexagonal cells as shown in Figure 11, and the surface averaged fluxes are approximated from the fluxes in these circular regions.

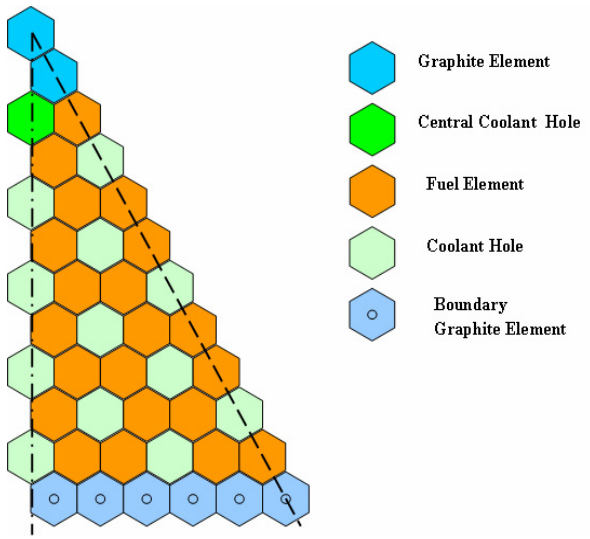

Figure 11. Fuel Block Model for DF Calculation in DRAGON.

The DFs that have been obtained for fuel blocks with or without burnable poisons (BPs) are plotted in Figure 12. Burnable poisons are loaded in the six corner holes as shown in Figure 3. For a fuel block without BPs, fast group DFs are smaller than unity because fast group fluxes at the peripheral graphite region are smaller than the block average fluxes, and thermal group DFs are larger than unity due to increased neutron thermalization in the boundary region. For a fuel block with BPs, however, thermal group fluxes at the block boundary are smaller than the block average ones due to the flux depression by BPs loaded in the six corner holes. Verification of the cross section generation with single fuel block calculations will be further discussed in the following sections. Fuel blocks with inserted control rods are also discussed later.

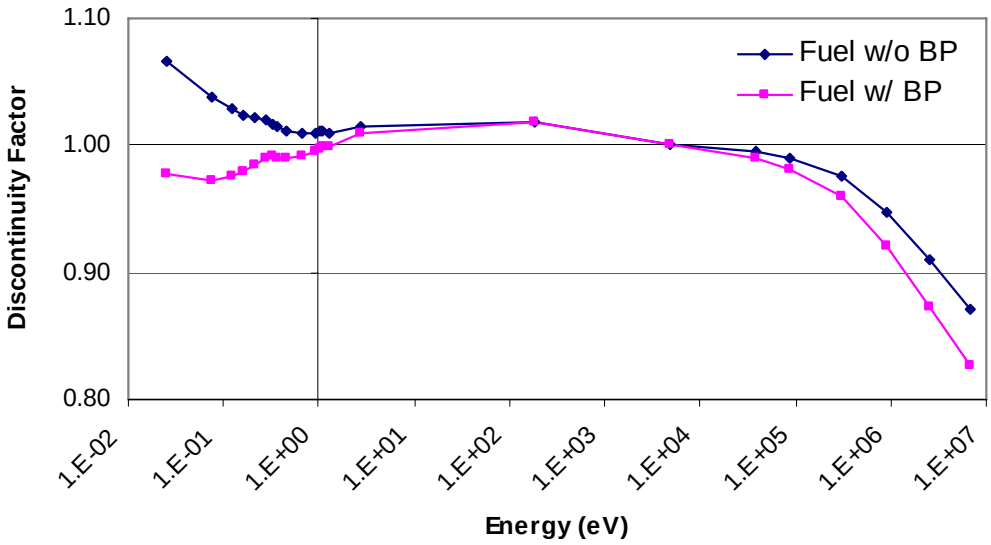

Figure 12. Comparison of 23-Group DFs for Fuel Blocks With and Without BP.

2.4 Reflector Cross Sections

The fast neutrons leaking into the inner and outer reflectors are slowing down in the reflector and return to the core as thermal neutrons, and thus high power peaks can develop at the core-reflector interfaces. The thermal neutron current from the reflector to the core makes the neutron spectrum change significantly from the core-reflector interface to the other side of the assembly. To model this spectral transition accurately, the cross sections of fuel blocks located at the core-reflector interface can be generated separately using multi-block calculations. However, this approach makes the cross section generation procedure much more complicated. Therefore, it was decided to use the single block calculation approach for fuel block cross section generation and account for the spectral transition effects in the reflector cross sections generation.

Radial Reflector Model

Reflector cross sections could be generated by simple energy-group collapsing with the fine-group spectra obtained from the lattice physics calculation for a multi-region (fuel and reflector) problem. However, since the thermal spectrum changes significantly at the interface region between the core and reflector, the reflector cross sections for the homogeneous, multigroup problem need to be adjusted using the equivalence theory to preserve reaction rates and currents of the original heterogeneous, fine-group problem.

In this work, a model to generate effective reflector cross sections is developed and analyzed, based on simplified one-dimensional (1-D) spectral fuel-reflector geometry to represent the actual core. Initially, a hexagonal cell in the fuel region is converted to a rectangular one by preserving each material volume, as shown in Figure 13.

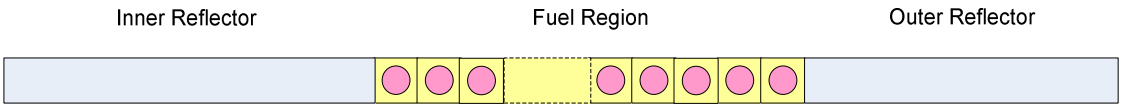

Figure 13. Two-Dimensional Core Slice Model.

However, it was found that the DRAGON solution for the fuel-reflector problem with rectangular-cell geometry is not correct, compared to the MCNP reference results. Therefore, the hexagonal pin-cell geometry was changed to the slab-cell shown in Figure 14. The fuel and cell widths were adjusted such that the fuel-to-moderator volume ratio and the multiplication factor are preserved. The fuel and cell widths are respectively 0.597 cm and 2.082 cm for a fuel-cell with homogeneous fuel compact model, and 1.012 cm and 3.528 cm for the heterogeneous fuel compact model with explicit TRISO particle representation. For the verification test here, a fuel-cell with homogeneous fuel compact model was used.

The three-region (reflector-fuel-reflector) problem was further simplified to a two-region (fuel-reflector) model shown in Figure 14, based on the observation that the results change very little as far as the reflector size is greater than twice the block pitch. A reflective boundary condition was used at the outer boundary of the fuel region, for both the outer and inner reflector models. A reflective boundary condition was employed at the outer boundary of the reflector region of the inner reflector model, and a vacuum boundary condition is applied for the outer reflector model.

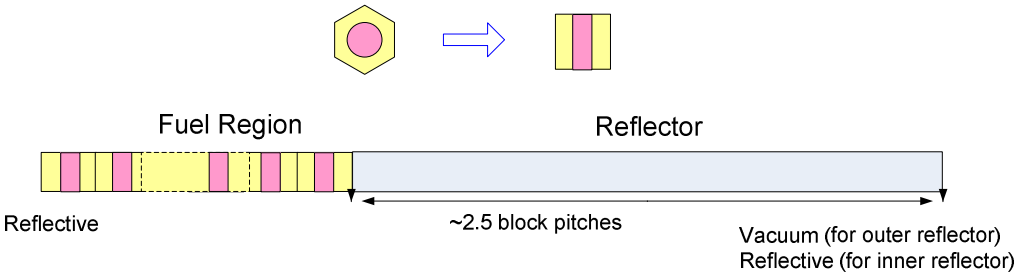

Figure 14. Simplified One-Dimensional Slab Fuel-Reflector Model.

A reference solution was first calculated with DRAGON using the heterogeneous geometry, and then spatial homogenization and group collapsing were performed separately for the fuel and reflector regions. A finite difference method (FDM) code was programmed to obtain the homogeneous surface fluxes at the fuel-reflector interface. A fixed source problem was solved with the boundary current sources specified at both ends, which were determined from the reference DRAGON solution. Discontinuity factors at the interface were calculated by comparing the homogenous surface fluxes obtained from the FDM solution and the heterogeneous surface fluxes of the reference DRAGON solution. Using the homogenized cross sections, DIF3D calculations were performed using the nodal-diffusion option, which is based on a fourth-order nodal expansion method with transverse leakage approximations.

Table 7 compares the multiplication factors from DRAGON and DIF3D calculations. The 69-group DIF3D results agree well with those of DRAGON, while the 23-group DIF3D results without DFs show a difference of 300 ~ 400 pcm. This indicates that in this fuel-reflector model, the energy spectrum effect is more pronounced than the spatial homogenization effect. The 69-group results suggest that the transport effect is very small. When DFs are applied to the 23-group problem, the DIF3D result is significantly improved and agrees well with the reference DRAGON result. This implies that the discontinuity factor based on the equivalence theory works very well for the fuel-reflector problem.

The surface fluxes at the interface between fuel and reflector regions determined with and without DFs are compared in Figure 15. As can be seen, the introduction of DFs significantly improves the accuracy of surface-average fluxes. The surface-average fluxes obtained by the nodal diffusion option of DIF3D with DFs agree very well with the DRAGON results within ~1%.

Table 7. Comparison of DRAGON and DIF3D Multiplication Factors for 1-D Fuel-Reflector Model without Control Rod

Code		Type A (inner)		Type B (outer)	
		k-inf	Δk (pcm)	k-inf	Δk (pcm)
DRAGON, 69 g		1.43483	-	1.37084	-
DIF3D (Nodal diffusion)	69 g (w/o DF)	1.43528	45	1.37173	90
	23 g (w/o DF)	1.43826	343	1.37454	371
	23 g (w/ DF)	1.43497	14	1.37082	-2

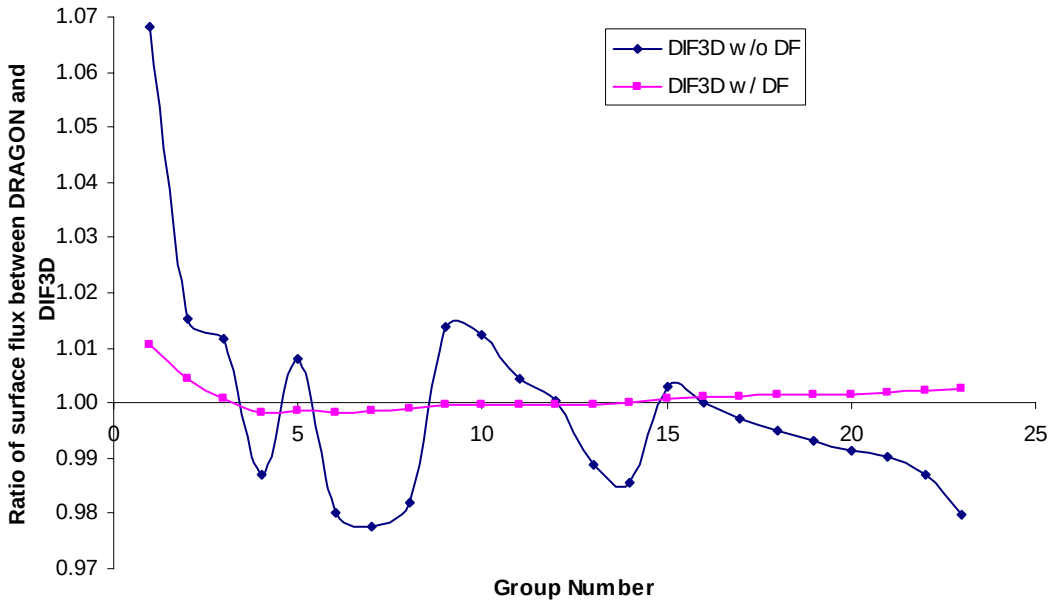

Figure 15. Comparison of Surface Fluxes at Interface between Fuel and Reflector.

Axial Reflector Model

Axial reflector cross sections can be generated in the same way as the outer radial reflector cross sections. This is reasonable since both the axial and outer radial reflectors have the same vacuum boundary condition (different reflector thickness). It is also observed that reflector cross sections and DFs at the fuel-reflector interface change very little as long as the reflector size is greater than a certain length (about two-block pitch).

When the cross sections are based on the simplified equivalence theory, the DFs are implicitly applied to all directions including the axial direction. The DFs between two adjacent axial nodes of the fuel block canceled out, since fuel blocks are homogeneous in the axial direction. However, DFs remain active at the fuel-axial reflector interface because the values for fuel and reflector blocks are not the same. This could lead to an over-correction of the leakage. In order to deactivate DFs of the fuel region even at the fuel-reflector interface, the DFs of axial reflector cross sections can be modified to $f_{reflector} \cdot f_{fuel}$, where f_{α} is a discontinuity factor of region α. Of course, this is not an issue when the surface-dependent DFs based on the nodal equivalence theory are assigned separately.

2.5 Control Rod Cross Sections

Control Rods in Reflector Region

In order to model control rod insertion in the outer reflector region accurately, the 1-D slab geometry used for reflector cross section generation was re-examined. The control rod was transformed into a thin slab, whose width was determined to keep the same volume ratio of control rod to graphite in the original two-dimensional geometry. The reflector slab size was set to 36 cm and the control rod slab size was adjusted to 2.6 cm. For the purpose of testing the homogenization effect of strong absorber, the control rod slab was placed at 4 cm from the interface of the fuel and reflector regions (see Figure 16).

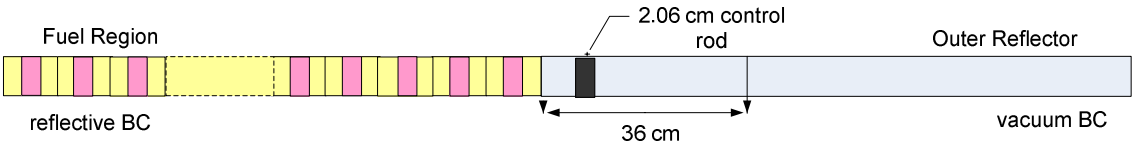

Figure 16. One-Dimensional Slab Geometry Model for Control Rod.

For this one-dimensional problem, a fine-mesh DRAGON calculation was performed with the 172-group library, and homogenized 23-group cross sections were generated for three regions: fuel, rodded reflector and remaining reflector regions. Discontinuity factors were also calculated using the one-dimensional FDM code with boundary current sources derived from the DRAGON result. A DIF3D calculation for the three-region problem was then performed using these group constants. Due to the strong heterogeneity with a control rod in the reflector region, DFs are essential to preserve the currents at the fuel-reflector interface. The results in Table 8 indicate the importance of DFs, showing a significant error reduction when DFs are applied for the reflector side.

Table 8. Comparison of DRAGON and DIF3D Multiplication Factors for 1-D Fuel-Reflector Model with Control Rod.

Code		k-inf	Δk (pcm)
DRAGON, 172 g		0.92675	-
DIF3D, 23g	w/o DF	1.00342	7,667
	w/ DF	0.93250	575

As shown in Figure 17, the introduction of DFs improves the accuracy of surface-average fluxes noticeably. When a strong thermal absorber loaded closely to the fuel region is homogenized without discontinuity factors, the homogeneous thermal group fluxes are overestimated at the interface and thus the thermal absorption at the interface is underestimated. This large error in thermal group fluxes is almost eliminated by applying DFs.

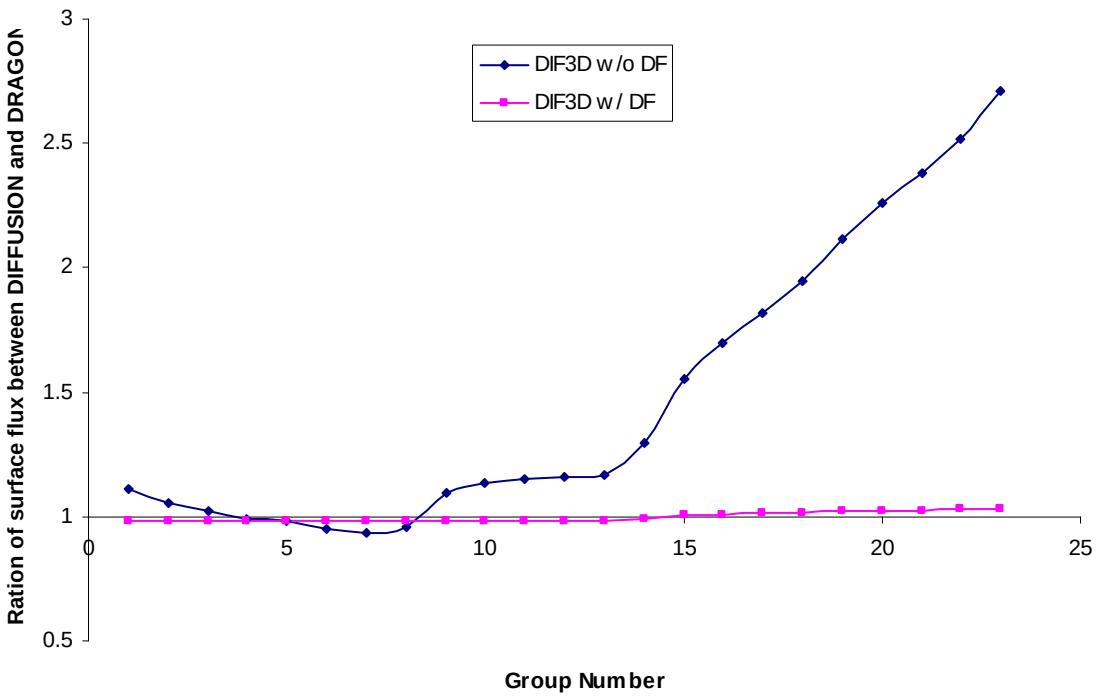

Figure 17. Comparison of Surface-Average Fluxes at Interface between Fuel and Rodded Reflector with and without DFs.

To test the control rod cross sections generated from the one-dimensional model discussed above, 2-D VHTR benchmark problems were prepared and solved with both DRAGON/DIF3D and MCNP. Preliminary results showed that control rod worths are significantly overestimated with these control rod cross sections. This appears to be due to incorrect control rod width and distance from a fuel block used in the one-dimensional geometry model. It is difficult to represent the control rod asymmetrically inserted in a block accurately by a 1-D model, thus a two-dimensional control rod model (two-ring core with reflective boundary condition) was developed to generate control rod cross sections for the reflector region.

Since control rods are asymmetrically inserted in fuel or reflector elements of the prismatic VHTR core, surface-dependent adjustment factors for homogenized cross-sections need to be introduced to model the power tilt of rodded regions correctly. Figure 18 illustrates the two-dimensional models used for generating control rod cross sections in the reflector region. Since the current version of DRAGON cannot solve accurately two-dimensional (2-D) multi-block problems with fuels and reflectors, the MCNP code was used to solve the problem. However, it is difficult to generate all the cross sections (including transport and scattering cross sections) with sufficiently small statistical error directly from MCNP solutions. Therefore, two calculation options were investigated.

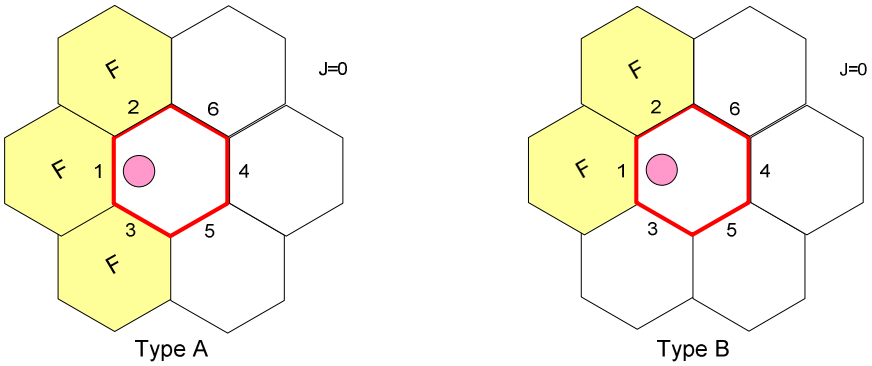

Figure 18. Two-Dimensional Modeling for the Rodded Reflector Region.

The first option is to use the 1-D fuel-reflector model corresponding to the two-dimensional seven-assembly model and determine the control rod position iteratively such that the control rod worth determined from DRAGON/DIF3D solutions is equal to that of 2-D MCNP solution. Reflective boundary condition is used when searching for the location of control rods in the 1-D problem. Once a control rod location is determined in the slab geometry, the cross sections of rodded reflector block are re-generated using the solution of the 1-D slab problem with vacuum boundary condition. Figure 19 illustrates the procedure. This option is advantageous because of its simplicity and the applicability of the existing 1-D procedure, but it does not provide surface-dependent discontinuity factors. Using the iterative process, the distance of control rod from the fuel-reflector interface was determined for the 1-D slab models corresponding to the two seven-block models shown in Figure 18. The determined distance was 14.857 cm for Type A and 13.490 cm for Type B. The width of control rod slab is 2.06 cm for

both types, which is determined to keep the original volume ratio of reflector to control rod. It is noted that the control rod worth of Type B is larger than that of Type A due to more thermalization from a larger volume fraction of graphite in the zone. Thus, control rod cross sections for Types A and B are separately generated.

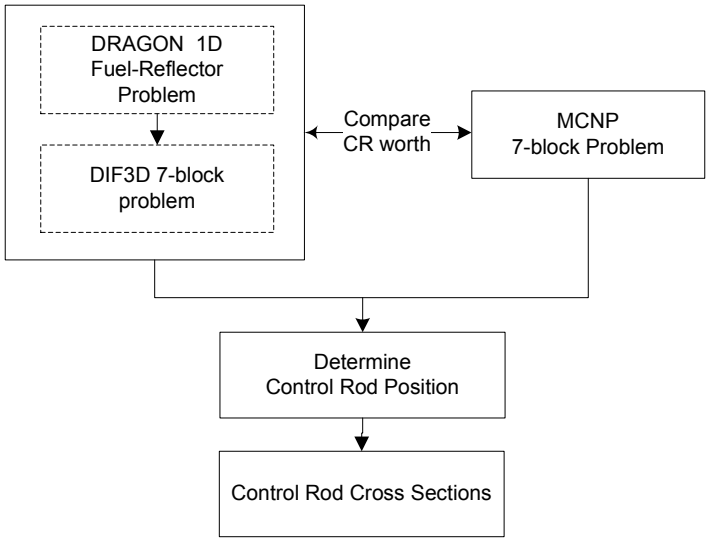

Figure 19. Generation of Control Rod Cross Sections (Option A).

As seen in Table 9, the control rod worths of 172-group DRAGON/DIF3D 7-block calculations match well those from MCNP calculations since they are forced to be very close. The fuel and reflector cross sections were generated from the single block and one-dimensional fuel-reflector configurations, respectively. The control rod worths obtained from 23-group DRAGON/DIF3D calculations show some minor deviations because of group collapsing errors.

Table 9. Control Rod Worths of 7-Block Cores from MCNP and DRAGON/DIF3D

7 Block Core Type	Code	Energy Group	Multiplication Factor		CR Worth (%Δρ)
			w/o CR	w/ CR	
Type A	MCNP		1.45929 (±0.00029)	1.10594 (±0.00031)	21.89
	DRAGON/ DIF3D	172	1.45877	1.10685	21.80
		23	1.45827	1.11014	21.50
Type B	MCNP		1.38663 (±0.00025)	1.00875 (±0.00031)	27.02
	DRAGON/ DIF3D	172	1.38067	1.00407	27.17
		23	1.38081	1.00974	26.61

The second option is also a two-step procedure in which the region-wise average fluxes, surface fluxes, and currents are derived from MCNP solutions. The MCNP flux data are used in the DRAGON code to determine the homogenized cross sections of the rodded reflector block. For this, the DRAGON code has been modified to read region-wise fluxes from an external file. The FDM code calculates the discontinuity factors using the MCNP surface fluxes and currents. Based on trapezoidal meshes, the one-dimensional FDM code solves a fixed source problem with boundary current sources and transverse leakage approximations to obtain the homogenous surface fluxes of rodded reflector block:

$$J_R\, h_R - J_L\, h_L + \Sigma \phi A = -\left(J_T - J_B\right) l_{TB}\,, \tag{4}$$

where J_s = current at surface s (R : right, L : left), h_s = height, l_{TB} = length at top (T) and bottom (B) for trapezoid, and A = trapezoid area. In this work, a constant transverse leakage approximation is used for each half hexagon.

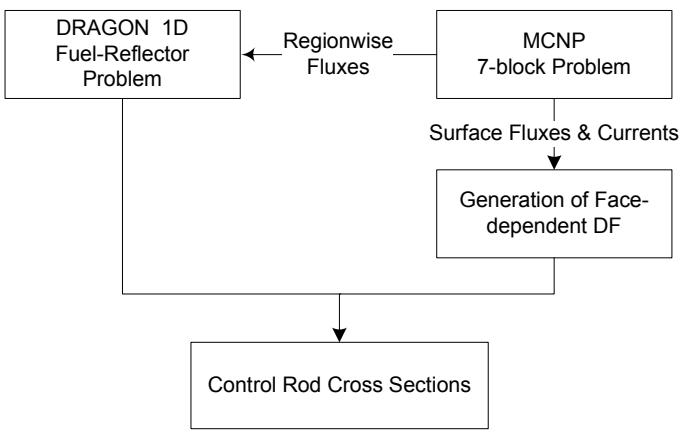

Figure 20. Generation of Control Rod Cross Sections (Option B).

The option B has a few issues related to its accuracy. One is the statistical uncertainties of the MCNP fluxes and currents, especially in high energy groups. Since the FDM solution is sensitive to the MCNP currents, the statistical uncertainties of the DFs are significant. Another issue is that the accuracy of the 1-D FDM solver can be degraded due to the flat transverse approximation. This can be improved in the future with a second-order or higher approximation. Finally, as aforementioned, the surface-dependent DF capability of DIF3D is available only for the nodal diffusion option, but it was observed that this solution option does not provide sufficient accuracy for VHTR rodded cores. In this work, therefore, the investigation of this

second option is limited to demonstrating the possibility to correct power sharing by applying surface-dependent DFs when control rods are asymmetrically loaded in the reflector block.

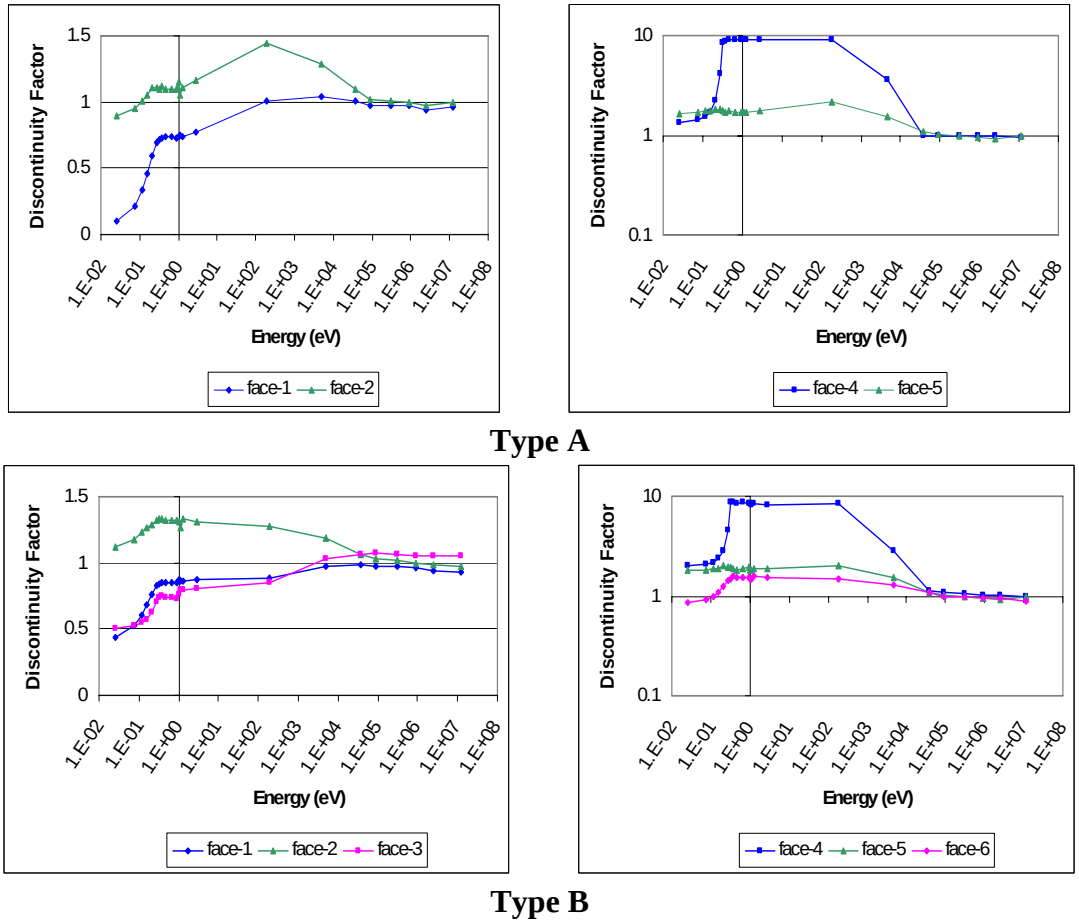

Type A

Type B

Figure 21. 23-Group Surface-Dependent Discontinuity Factors of Seven-Block Rodded Models.

Figure 21 shows the surface-dependent DFs of the two seven-block models (Types A and B) in Figure 18. As expected, the homogeneous surface fluxes of low-energy groups are larger than the heterogeneous fluxes at the surface close to the control rod (Face-1) and smaller at the opposite surface (Face-4) due to the homogenization of a small area of strong absorber to the whole region. Since the Face-2 is also relatively far from the control rod, the homogeneous fluxes of low-energy groups are smaller than the heterogeneous ones. Unlike the Faces-1 and -2, the Face-3 of Type B is a reflector-reflector interface. The flux on this surface is strongly influenced by the flux on the surface facing a fuel block. Due to the uncertainties of MCNP flux and current solutions, very large DFs are observed, especially at the surface (Face-4) which is the

farthest from the control rod. The values of the DFs were limited to 10 for the stability in the DIF3D-nodal calculations.

The control rod cross sections generated from the option B were used for the seven-assembly model (Type A) calculations to investigate the improvement in power distribution. In order to use surface-dependent DFs, the nodal diffusion option of DIF3D was employed with the DFs supplied through the DISFAC binary file. The application of surface-dependent DFs reduced the error in fuel block powers significantly as shown in Figure 22, but it increased the multiplication factor error slightly because of the combined effects of various uncertainties and approximations. To improve the accuracy, it would be desirable to (1) use a deterministic code instead of MCNP to analyze the characteristic seven-block models for homogenization, (2) improve the accuracy of the spatial approximation of the DIF3D-nodal option or implement the DFs into the nodal transport option VARIANT, and (3) enhance the accuracy of the FDM solver with better transverse approximations.

Table 10. Multiplication Factor and Rod Worth of Seven-Block Model (Type A).

Configuration	Code	k-inf	Rod Worth (%Δρ, pcm)
Seven-block model w/o CR	MCNP	1.45929 (±0.00026)	-
	DIF3D – Nodal w/ DF (23-g)	1.45548	-
Seven-block model w/ CR	MCNP	1.10594 (±0.00031)	21.89
	DIF3D – Nodal w/ DF* (23-g)	1.09975	22.22

* Face-dependent discontinuity factors applied to the rodded reflector block

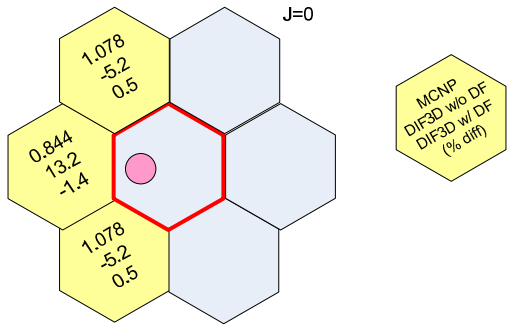

Figure 22. Power Comparison between MCNP and DRAGON/DIF3D for 2-D Seven-Block Model.

Control Rods in the Fuel Region

The control rods in fuel blocks are used for core shutdown. Therefore, accurate control rod cross sections are very important for safety analysis. The control rod has an annular shape with a hole at the center, and a gap exists between the control rod and graphite block. However, due to the geometry modeling limitation of DRAGON, the control rod and associated gaps and graphite in a fuel element need to be represented approximately in DRAGON calculations. In this study, they are approximately represented by multiple rings of pin-cell sized hexagons such that the amounts of graphite and other materials in the whole block are preserved.

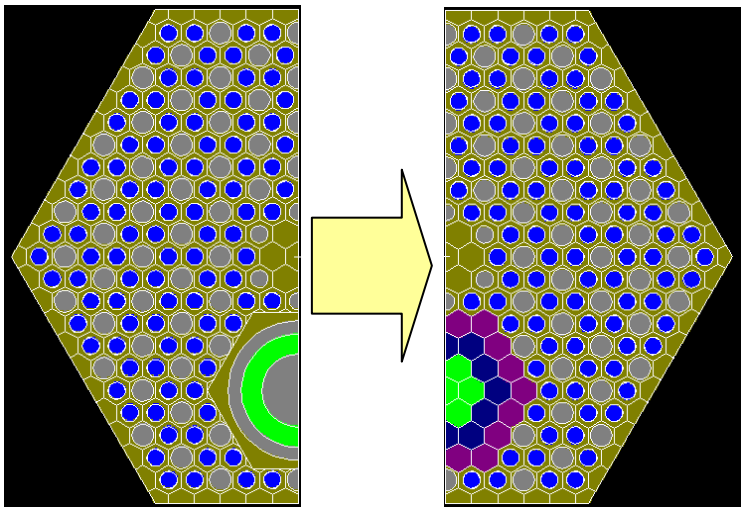

(A) Original Geometry (B) Approximate Geometry

Figure 23. Geometry Approximation of Rodded Fuel Block Model.

To preserve the k-infinity of the two different geometry models, the control rod zone represented by multiple rings of hexagonal cells was divided into three sub-zones, and different nuclide number densities were assigned to each sub-zone, as shown in Figure 23. In the actual geometry, the hole for the control rod is 10.16 cm in diameter, and the annular control rod is located 9.756 cm away from the center of the fuel block. The control rod has an inner diameter of 5.28 cm and an outer diameter of 8.26 cm. The number densities of B-10, B-11, and graphite of a control rod are 1.05773E-03, 1.06891E-04, and 6.02052E-02, respectively. In the approximate geometry shown in Figure 23(B), the control rod material is homogenized in three hexagonal rings, where the number densities of B-10, B-11, and graphite are increased by 26.6% for the two

inner rings and decreased by 15.5% for the outer ring to keep the multiplication factor close to that of the original geometry. Comparisons of the MCNP results for these two different geometry models showed that the differences in the k-infinity of rodded fuel block are -166 pcm and -95 pcm for the homogeneous fuel compact and the heterogeneous fuel model with explicit representation of TRISO particles, respectively.

The accuracy of control rod modeling with DRAGON was examined. For fuel blocks with a strong absorber, DRAGON requires to use the EXCELT option (the full collision probability tracking [14]) in order to obtain accurate solutions. However, it does not support the use of the EXCELT option for explicit coated fuel particle representation (i.e., TRISO particles). Therefore, a hybrid method using both SYBILT and EXCELT options was investigated to treat the double heterogeneous fuel compact in control rod models: a hexagonal fuel cell with explicit representation of TRISO particles is first solved using the SYBILT option (the collision probability for cells and current coupling between cells), and then the homogenized fuel cell cross sections are used for the fuel block calculation with the EXCELT option. A half-symmetry option (S180) was used for the rodded block calculation in DRAGON.

The results in Table 11 show that the DRAGON k-infinity differs from the MCNP result for the original geometry by -1706 pcm for the homogeneous fuel compact model and -608 pcm for the heterogeneous fuel compact model. For the heterogeneous fuel compact model, the difference becomes smaller because the overestimation of k-infinity by DRAGON for explicit TRISO particle representation is canceled out with the underestimation of that for the rodded fuel.

Table 11. Comparison of MCNP and DRAGON Multiplication Factors for Rodded Fuel Block.

Fuel Configuration	CR Geometry	Code	k-inf	Δk, pcm
Homogeneous Fuel Compact	Original (A)	MCNP	0.74022 (±0.00029)	Reference
	Approximate (B)	MCNP	0.73856 (±0.00030)	-166
		DRAGON	0.72362	-1706
Explicit TRISO Particles	Original (A)	MCNP	0.76803 (±0.00031)	Reference
	Approximate (B)	MCNP	0.76708 (±0.00031)	-95
		DRAGON	0.76195	-608

2.6 Energy Group Study

Previous studies at Argonne have shown that VHTR analyses require more energy groups than conventional LWR analysis because the spectral interactions between fuels and fuel and reflector are significant due to a much longer neutron mean free path. In this work, the number of energy groups versus accuracy has been studied using the one-dimensional fuel-reflector problem discussed previously, so that it would be a basis for energy group optimization in the future.

The previous results indicated that if cross sections are condensed with the correct flux spectrum and correct discontinuity factors are utilized, the reaction rates and currents can be preserved and an accurate estimation of the multiplication factor can be obtained. In the real situation, however, the spectrum cannot be known beforehand. As discussed earlier, fuel block cross sections are normally generated from a single fuel block calculation with reflective boundary condition, assuming that the spectrum of the single block configuration is not much different from the actual one in the core. The effects of energy group structure on the accuracy of homogenized nodal cross sections were examined by changing the number of energy groups from 4 to 23 groups as listed in Table 12, some of which have the same number of groups with different energy boundaries.

For simplicity, the homogenized fuel compact model was used. The 172-group cross section library was utilized for reference DRAGON calculations, and all the cross sections were generated at 300 K. Discontinuity factors for fuel and reflector cross sections were calculated based on the procedures discussed in Sections 2.3 and 2.4.

The results in Table 13 reveal several important points: (1) DFs can significantly reduce the homogenization errors for all energy-group structures, (2) the cross sections and DFs generated from a single fuel block calculation work very well for all energy groups, (3) the number of energy groups should be more than 4 groups, and 7 or more energy groups would be sufficient for uranium fueled VHTR, and (4) the accuracy is sensitive to the energy group boundaries. The 8(b) and 14(b) group structures, which show good performance, have more energy groups in the resonance regions, compared with the 8(a) and 14(a) group structures. Although the 4(a) group result has relatively small difference from the DRAGON reference solution for the inner reflector model, it still shows a large error in the outer reflector model.

Table 12. Choice of Energy Group Boundaries.

(Unit: eV)

23	14(a)	14(b)	8(a)	8(b)	7	4(a)	4(b)
3.679E+06	3.679E+06						
1.353E+06	1.353E+06					1.353E+06	
5.000E+05	4.979E+05	5.000E+05		5.000E+05	5.000E+05		
	1.832E+05						
1.110E+05		1.110E+05					
6.738E+04	6.738E+04	6.738E+04					
	2.479E+04						
9.118E+03	9.119E+03	9.118E+03		9.118E+03	9.118E+03	9.118E+03	9.118E+03
	4.540E+02			4.540E+02			
3.673E+02		3.673E+02	3.120E+02				
4.000E+00	4.000E+00	4.000E+00		4.000E+00	4.000E+00		
	2.380E+00						
1.500E+00							
	1.300E+00						
1.097E+00		1.097E+00	1.072E+00	1.097E+00	1.097E+00		
1.045E+00							
9.720E-01		9.720E-01					
8.500E-01		8.500E-01				8.500E-01	8.500E-01
	6.250E-01						
5.000E-01		5.000E-01	5.300E-01	5.000E-01	5.000E-01		
4.000E-01							
3.500E-01		3.500E-01	3.577E-01				
3.000E-01							
2.500E-01							
1.800E-01							
1.400E-01		1.400E-01					
	1.200E-01						
1.000E-01			1.116E-01	1.000E-01	1.000E-01		1.000E-01
5.000E-02		5.000E-02	5.692E-02				
			2.049E-02				

Table 13. DRAGON and DIF3D Multiplication Factors for Energy Group Study.

DIF3D (Nodal diffusion) Group	Inner Reflector Model DRAGON, k-eff = 1.40629		Outer Reflector Model DRAGON, k-eff = 1.36594	
	Δk (pcm)		Δk (pcm)	
	w/o DF	w/ DF	w/o DF	w/ DF
172	565	-13	567	62
23	683	71	901	99
14(b)	815	33	989	92
8(b)	684	-79	892	-20
7	837	-47	1053	22
4(b)	523	-416	845	-239
4(a)	1332	95	1738	297
8(a)	1508	-331	-	-
14(a)	515	-148	-	-

The same calculations were repeated for the one-dimensional fuel-reflector problem with a control rod. Reflector and control rod cross sections were generated as discussed in Sections 2.4 and 2.5, but fuel cross sections were generated with different collapsing spectra. Since the multiplication factor of the 1-D problem with control rod, 0.90958 (relatively harder spectrum), is closer to unity than the multiplication factor of fuel block, 1.47522 (relatively softer spectrum), the critical spectrum (relatively harder spectrum) were used for group collapsing. As shown in Table 14, when 172 group cross sections were used, the multiplication factor errors were reduced from 5840 pcm to 451 pcm by using DFs. Other group solutions are also significantly improved with the application of DFs, but the error of the 4-group solution is still larger than those of the other solutions. Results also lead to the same conclusion that the number of energy groups should be greater than four for VHTR core analysis.

Table 14. Comparison of Control Rod Worths with Different Number of Energy Groups.

DIF3D (Nodal Diffusion)		Outer Reflector Model with CR DRAGON, k-eff = 0.90958	
		Δk (pcm)	
		w/o DF	w/ DF
Fuel cross sections generated with single fuel block spectrum	172 g	5840	451
	23 g	6027	685
	14(b) g	6189	714
	8(b) g	6270	774
	7 g	6332	861
	4 g	6781	1258

2.7 Pin Power Factors

In the state-of-the-art methods for thermal reactor analyses, the pin power distributions are usually estimated by superposition of pin power form functions derived from single fuel assembly calculations on the homogenous power distribution determined from a whole-core calculation. The RCT code [15] developed at Argonne has a capability for calculating homogenous fluxes and power shapes within a fuel assembly using the assembly-average and surface-average data obtained from DIF3D nodal diffusion calculations. Since it was developed for fast reactor application, however, it does not use pin power form functions. For the pin power reconstruction of VHTR fuel blocks, pin power factors of each fuel block type were derived from DRAGON calculations. Since the current version of DRAGON does not provide the pin power edits, its output routine was modified to edit relative pin powers, using the pin map in the "CELL" input of the code.

Pins were numbered in a way consistent with the pin numbering sequence used in the flux and power reconstruction of the RCT code and were saved in a full-block format to an external file regardless of the DRAGON input for symmetry options. Using the pin numbering scheme shown in Figure 24, pin powers were generated from the DRAGON calculation as illustrated in Figure 25.

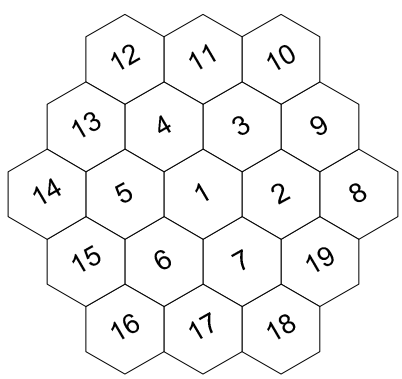

Figure 24. Pin Indexing for Hexagonal Geometry.

Pin powers were calculated for the standard VHTR fuel block using DRAGON and compared with reference MCNP results. The power variation among fuel pins is up to 4 % and the peak power occurs at the fuel block corner due to relatively large amount of graphite in this

zone. The pin powers are shown to have good agreement between MCNP and DRAGON. The maximum error of 1.3% occurs at the corner pin.

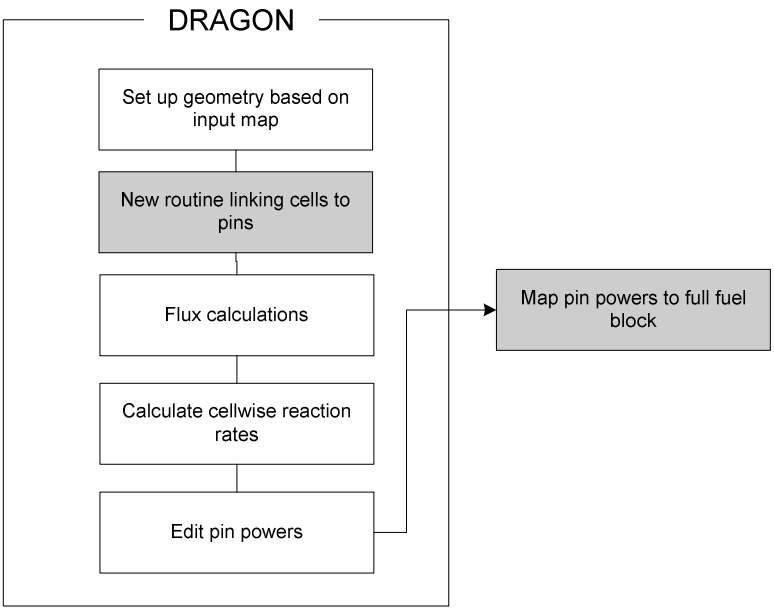

Figure 25. Process for Generating Pin Power File in DRAGON.

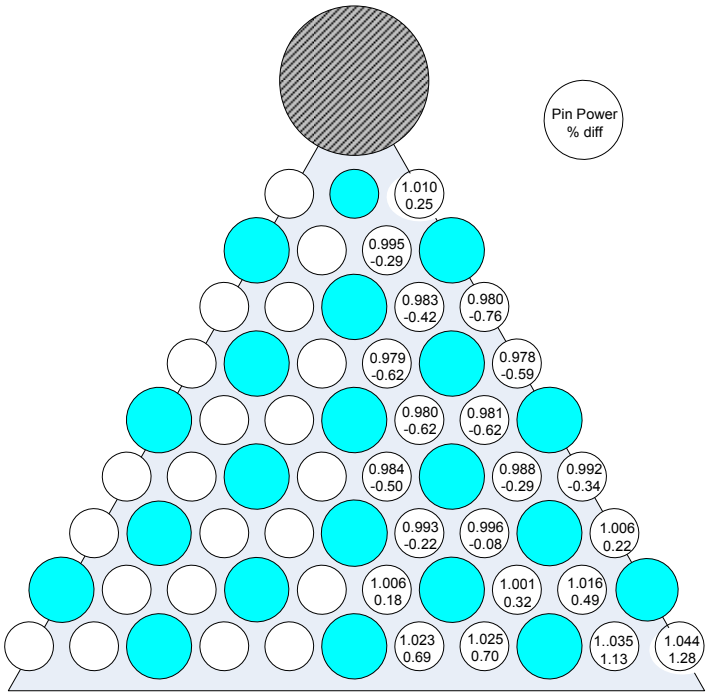

Figure 26. Pin Power Distribution Determined from DRAGON Calculation.

3.0 X-MANAGER

As discussed in the previous sections, cross section generation requires many DRAGON calculations: fuel block depletion with fuel and moderator temperatures, 1-D fuel-reflector calculations with reflective or vacuum boundary conditions, and the coupling of 1-D fuel-reflector calculations using DRAGON, 2-D seven-block calculations by MCNP and so on. Anticipated output data from DRAGON calculations include discontinuity factors (DFs) and pin power factors, along with ISOTXS-format files containing cross sections.

For routine design, a large number of DRAGON depletion jobs are run with a possible range of fuel and moderator temperatures for all components in the core of interest. These include fuel blocks with or without burnable poisons or control rods and reflector cross sections (inner, outer, top, and bottom) with or without control rods. DRAGON produces a separate cross section file in an ISOTXS format for each calculation step, which means that a large number of ISOTXS files are created to prepare cross sections for the REBUS-3/DIF3D core calculation. However, since REBUS-3 accepts only one ISOTXS file during each calculation, the multiple ISOTXS files have to be merged into a single file named ISOTAB which is organized to efficiently represent burnup and temperature changes. In addition, many of the fission products from DRAGON depletion calculations are lumped into one representative *lumped fission product* to save both data size and computation time. Discontinuity factor and pin power factor files are also generated using DRAGON outputs and small programs developed in this work. These data are also merged into one file for each type.

The fuel block depletion is performed at different temperature conditions. Since the history effect due to temperatures is found to be much smaller than the effect from the instant temperature change, no restart calculation is needed for different temperature conditions. However, a control rod in the fuel block is modeled separately for restart cases at selected burnups because the history effect due to such a strong neutron absorber is not negligible. Control rod cross sections are generated only at average temperature condition, assuming that their change due to the temperature variation is relatively very small. This assumption is also applied to pin power factors and discontinuity factors, which accordingly are generated only at

average temperature condition. Reflector cross sections are created from the one-dimensional fuel-reflector problem as discussed in the previous section.

Once ISOTXS, DF, and pin power factor files are created for all required conditions, they are merged into one file for each type that can be read by REBUS-3/DIF3D. As discussed in Section 2.1, cross sections are tabulated in terms of burnup, moderator and fuel temperatures in an ISOTAB format which has a hierarchical structure with isotope, burnup, and temperature. Control rod cross sections are treated as an isotope but using a delta-macroscopic format:

$$\Delta\Sigma_{\alpha g} = \Sigma_{\alpha g}^{rodded} - \Sigma_{\alpha g}^{unrodded},$$

where g = group, α = cross section type. Delta-macroscopic cross sections for control rod are defined by subtracting unrodded macroscopic cross sections from rodded ones. When a control rod is inserted, delta-macroscopic cross sections are simply added to the final macroscopic cross sections based on flux and volume weighting. Figure 27 summarizes how cross sections are processed from DRAGON to REBUS-3/DIF3D.

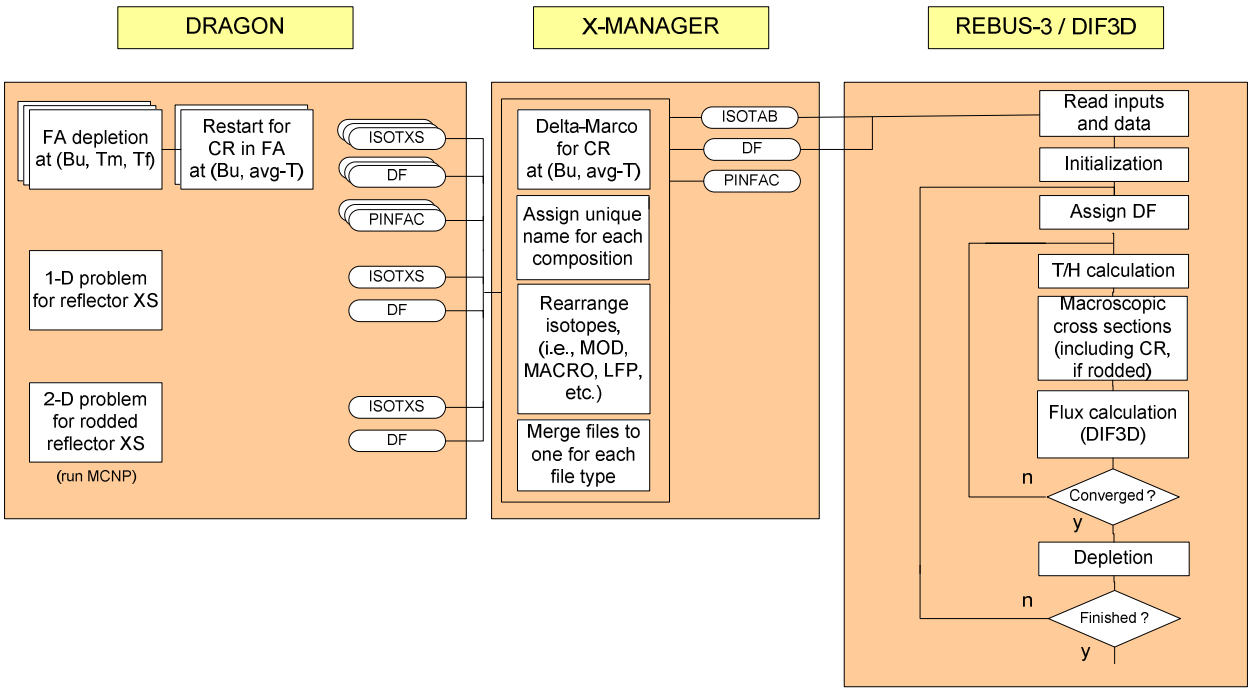

Figure 27. Data Flow for DRAGON, X-MANAGER, and REBUS-3/DIF3D.

The procedure for cross section generation with DRAGON has been partially automated in X-MANAGER, which is a toolkit for efficiently managing cross sections. The toolkit, programmed with a UNIX shell script, is composed of many functions that use keywords for inputs, as shown in Figure 28.

In general, the functions read base data to provide necessary input, run executables if needed, and extract data from outputs for the next step. All default paths required for executables and libraries are stored in the toolkit, but they can be defined by a user. For example, multiple DRAGON jobs can be submitted by simply changing state parameters with keyword inputs:

```
Run_Dragon      Dragon_Inp=inp_dragon  Tf=1000  Tm=850 Tc=750            \
                Isotab_Inp=inp_isotab  Xs_Id=A  Save_Dir=$HOME/dragon
Run_Dragon      Dragon_Inp=inp_dragon  Tf=1000  Tm=950 Tc=750            \
                Isotab_Inp=inp_isotab  Xs_Id=A  Save_Dir=$HOME/dragon
Run_Dragon      Dragon_Inp=inp_dragon  Tf=1100  Tm=850 Tc=750            \
                Isotab_Inp=inp_isotab  Xs_Id=A  Save_Dir=$HOME/dragon
.
.
```

```
#-----------------------------------------------------------------------------------------------
# Call the X-MANAGER toolkit
#-----------------------------------------------------------------------------------------------
. /data/RA/dragon_rebus/XMANAGER/xmanager
#-----------------------------------------------------------------------------------------------
# Define executables, if different from default.
#-----------------------------------------------------------------------------------------------
DRAGON_LIB=/data/RA/jimdeen/wimslib.v6.172g.unix.jun02.mod.gz
DRAGON_EXE=/data/RA/DRAGON/DRAGON.june00.x
ISOTAB_EXE=
READ_ISOTAB_EXE=
READ_ISOTXS_EXE=
WORK_DIR=
#-----------------------------------------------------------------------------------------------
# Available functions
#-----------------------------------------------------------------------------------------------
Run_Dragon      {keyword: Dragon_Inp=, Tf=, Tm=, Tc= Isotab_Inp=, Xs_Id=, Save_Dir=,  Df_Lsurf=,
          Df_Rsurf=, Ext_Flux= Df=}
Merge_Isotxs    {keyword: File=, Id=}
Merge_Isotab    {keyword: Dir=}
Merge_Df        {keyword: Dir=}
Merge_Powform   {keyword: Dir=}
Read_Isotab     {keyword: Dir=}
Read_Isotxs     {keyword: File=}
Read_Df         {keyword: File=}
Create_Delcr    {keyword: Base_Isotab=, Crod_Isotab=}
Create_1dref    {keyword: Dir=, Xs_Id=}
```

Figure 28. Functions and Libraries of X-MANAGER.

Then, separate DRAGON jobs are executed simultaneously, producing an ISOTAB file for each job, in which all six-character isotope names are labeled, for example, with the character "A" (defined with the keyword "Xs_Id=") at the last character position and filled with "_" between an isotope name and "A" (e.g., U235_A, HE___A). A base input deck of DRAGON should be predefined for the geometry of concern, including indices, "/TFUEL/", "/TMOD/", and "/TCOOL/", for fuel, moderator, and coolant temperatures, respectively. If the keyword "Df=" is set to "on", cross sections are corrected with discontinuity factors based on the simplified equivalence theory. Otherwise, they remain uncorrected.

The ISOTAB, DF, and pin power files can be merged using the functions "Merge_Isotab", "Merge_Df", and "Merge_Pinform", respectively. With the multiple use of the keyword "Dir=", it is possible to search and merge files from many directories.

```
Merge_Isotab     Dir=$HOME/type_A  Dir=$HOME/type_B  Dir=$HOME/type_C  …
Merge_Df         Dir=$HOME/type_A  Dir=$HOME/type_B  Dir=$HOME/type_C  …
Merge_Powform    Dir=$HOME/type_A  Dir=$HOME/type_B  Dir=$HOME/type_C …
```

To define delta-macroscopic format control rod cross sections, two ISOTAB files are needed for the cases with and without control rod. Each ISOTAB file has macroscopic cross sections saved in the "MACRO" block. When "Create_Delcr" is called with the keywords "Base_Isotab=" and "Crod_Isotab=", delta-macroscopic cross sections are calculated by comparing MACROs from the two ISOTAB files and saved in the "CRODn" block in which "n" could be any single-digit number so that up to 9 different compositions can be defined for control rods.

As mentioned in Section 2, the generation of reflector cross sections requires a tedious process. Currently, one-dimensional fuel-reflector DRAGON inputs need to be manually provided for inner and outer reflectors, with a slab-type fuel equivalent to the original hexagonal super-cell. Once DRAGON generates an ISOTXS cross section file for reflectors, the function "Create_1dref" in X-MANAGER automates calculating equivalence parameters for the interface between fuel and reflector and then adjusts the cross sections with those parameters Other functions such as "Merge_Isotxs", "Read_Isotxs", "Read_Isotab", and "Read_Df" are supplemental, which may be needed when using the merged ISOTXS files for the direct use of DIF3D or examining the contents of files. More functions are under development, along with more warnings and error traps for user convenience and performance assurance.

4.0 SPATIALLY-HETEROGENEOUS CODE DEVELOPMENT

The ANL work on the development and validation of a capability for analysis of the prismatic VHTR/NGNP has focused in the short-term on the development of a deterministic code suite consisting of a lattice physics code and a nodal diffusion or transport code for efficient and accurate flux and power distributions and reactivity calculations. In order to efficiently accomplish the project goal, existing codes are being used as the basis of the new code suite with the addition of required functionalities for VHTR applications. The REBUS-3/DIF3D code system that was developed at ANL is the basis for this code suite development, as this code system has been used for the reactor physics analyses of fast reactors as well as LWRs. The DRAGON code has been used for the generation of cross sections.

In parallel to developing a suite of codes based on the conventional two-step lattice and whole-core calculation approach, it is important to envision and develop analysis tools for the future. These tools should eliminate the approximations inherent in the multi-step approach for whole-core analysis and be of higher accuracy and also less cumbersome to use. These attributes indicate that the future codes be based on a spatially-heterogeneous capability that eliminates the various stages used in current state-of-the-art tools. One obvious choice of a code would be that based on the stochastic Monte Carlo approach. The Monte Carlo techniques provide detailed solution of the neutron transport problem in space, energy, and angle and could be applied with great accuracy to the VHTR if fuel particles are modeled explicitly in the core calculation. The utilization of the Monte Carlo codes is however currently unattractive because of the tremendous problem size and the need for a large number of neutron histories required for resolution of fuel-element power distribution and small reactivity effects. Furthermore, several important phenomena such as thermal feedback at power generating conditions, flux uncertainty propagation in the depletion calculation and fission product build up are not properly addressed in these tools at the current time. In contrast, the direct three-dimensional whole-core transport calculation employing deterministic solution techniques provides a possibility for resolving all these problems as long as the double heterogeneity modeling capability is properly incorporated.

The development of advanced neutronics capabilities is ongoing in other USDOE projects. These codes would provide detailed spatially-heterogeneous, whole-core (3-D) transport

capabilities that eliminate the need for a separate cross section generation and homogenization step, functionalization of the cross section data, and interpolation of the cross-section data in a whole-core simulation code. Two potential code options are available at ANL for performing this task: the UNIC (pronounced "unique") capability that is being developed in-house or the DeCART code that has been developed under a joint US/ROK I-NERI project. This prismatic VHTR project has interacted with the code developers to ensure that the code capabilities are useful for VHTR/NGNP analysis; for either code, a capability for hexagonal block and double heterogeneity treatment would be required. In this section, the status of the DeCART and UNIC code pertinent to VHTR analysis are discussed.

4.1 DeCART Code Development at KAERI (ROK)

Background

The DeCART code [16] was originally developed for LWR applications at KAERI under a US/ROK I-NERI project led by ANL and KAERI, completed in early 2005. This code utilizes the method of characteristics (MOC) and eliminates the approximations and laborious multigroup constant generation stage of the two-step approach by representing local heterogeneities explicitly without homogenization, using a multigroup cross section library directly without group condensation, and incorporating pin-wise thermal-hydraulic feedback. The original DeCART code was developed to handle only rectangular fuel elements. To support the analysis of the prismatic VHTR, it was necessary to extend the geometrical capability to hexagonal fuel elements. This work has been started at KAERI under existing I-NERI collaborations with ANL, and the current status of that work was presented to ANL colleagues by *Dr. Kang-Seog Kim (KAERI)* at a recent project review meeting held August 10 and 11, 2006 at Argonne.

DeCART Code Status

The existing Cartesian geometry capability is being extended to hexagonal-Z geometry. The 3-D transport calculation method is based on a 2-D Method of Characteristics (MOC) solution approach coupled to an axial 1-D MOC transport or nodal diffusion solution. The major effort at this time has been devoted to the development and programming of the modular ray

tracing scheme for hexagonal fuel block. In this approach, the fuel block is sub-divided into small heterogeneous hexagonal cells on the scale of the fuel pin (compact) or coolant hole and surrounding graphite. This cell can be divided into tiny flat surface regions in which the variation of the neutron source consisting the fission and scattering sources as well as the cross sections are assumed constant. These flat regions are defined by concentric rings and azimuthal sectors. [16]

When a neutron ray passes through a flat source region, it would be augmented or attenuated according to the characteristics of the flat source region. There would be a change in the intensity between the incoming and outgoing rays of the region for the given angle. This change can be determined analytically by solving a simple neutron balance equation along the ray subject to the incoming boundary condition. The solution of this equation has two terms: the first term represents the attenuation term of the incoming beam, while the second term is the augmentation term due to the source generated within the region. The outgoing angular flux can be used as the incoming angular flux of the neighboring region and thereby the ray tracing can be continued until the physical boundary is reached. After the ray tracing is performed for all the discretized angular directions, the scalar flux of the flat flux region can be obtained as a weighted average of angular fluxes. This scalar flux can then be used to update the fission and scattering sources for use in the next ray tracing. [16]

The MOC calculation is conceptually very simple. However the actual implementation of a ray tracing capability into a code requires significant amount of coding and storage because it is necessary to determine the length and the flat flux region identification number for each ray segment. In order to mitigate the memory requirement, the so-called modular ray tracing scheme was developed by which the ray spacing and the azimuthal angles are slightly adjusted such the whole ray can be constructed by connecting several ray segments defined only for typical hexagonal blocks.

For the purpose of the intra-assembly ray tracing, 13 structure units have been identified and represented. These are shown in Figure 29. An assembly ray passes through the structure unit, and produces the cell rays on the structure units. The cell rays are gathered for the structure units, and cell analysis is performed based on the cell rays.

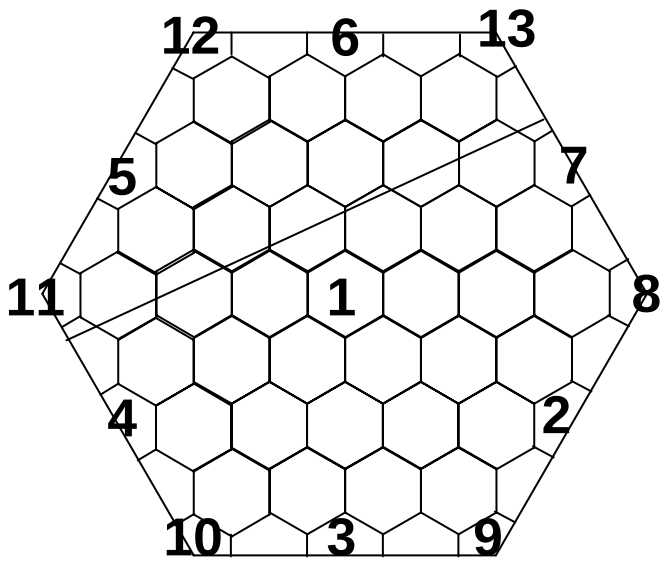

Figure 29. Structural Units of Hexagonal Assembly.

The hexagonal assemblies are linked to form the core layout. A so-called "dummy assembly" is defined at the outer boundary of the core, because the boundary is not necessarily hexagonal shaped. This assembly type is required for accounting for re-entering neutron and for specifying the albedo boundary condition.

This extension to hexagonal geometry has been completed and the code can now perform full-core problems and cases with 60° or 120° reflective symmetry. Work is ongoing to allow more symmetric boundary conditions (e.g., periodic boundary condition). The coarse mesh finite difference (CMFD) scheme to accelerate the spatial solution is also under development at this time. Additionally, the 1-D transport solution approach and the thermal-hydraulic modules that have been previously developed will be retained, with modification for hexagonal geometry. Finally, the subgroup method developed for the original Cartesian geometry code is being retained for resonance treatment.

With these features in place, DeCART would perform direct core calculations at power generating conditions. It does not require *a priori* group constant generation as is done in the two-step procedure, but accesses directly a multigroup cross section library to determine the cross sections corresponding to the local thermal condition. The temperature effect on the resonance cross sections is incorporated during the iteration process through the subgroup

method. This adaptive resonance calculation feature should be applicable to VHTR problems as well. In order to accomplish this feature for the fuel element, modifications are required in the fuel temperature and resonance calculation procedures, and would be completed in the future. An effective thermal feedback scheme for VHTR will thus be devised and implemented.

A major task that remains is the provision of a module for representing the heterogeneity effect arising from the use of the coated fuel particles in the graphite matrix. At the current time, this effect is being represented using the Reactivity Physical Transformation (RPT) that has been developed by KAERI. [17]

Preliminary Testing of DeCART Hexagonal Geometry Capability

Full and fractional assembly block problems and a 2-D, 1/6-core problem have been solved using the hexagonal geometry version of the DeCART code. These calculations were done using the RPT method for particle heterogeneity treatment. Table 15 summarizes the results for a fuel block with control rod hole at different operating temperatures. The schematic for this assembly is given as Figure 30. The DeCART solutions have been compared to MCNP results obtained using heterogeneous particle representation. The HELIOS code results using the RPT model have also been included for comparison (HELIOS is a vendor supplied code that has no double heterogeneity treatment).

Table 15. Comparison of DeCART and MCNP and HELIOS Results for VHTR Assembly.

Code	Parameter	300 K	600 K	900 K
MCNP (Heterogeneous particle treatment)	K-inf	1.54717	1.50096	1.46770
	(σ)	0.00051	0.00051	0.00045
HELIOS	K-inf	1.54806	1.50385	1.47092
	Δρ,pcm	35	128	149
DeCART	K-inf	1.54596	1.50140	1.46813
	Δρ,pcm	-51	20	20

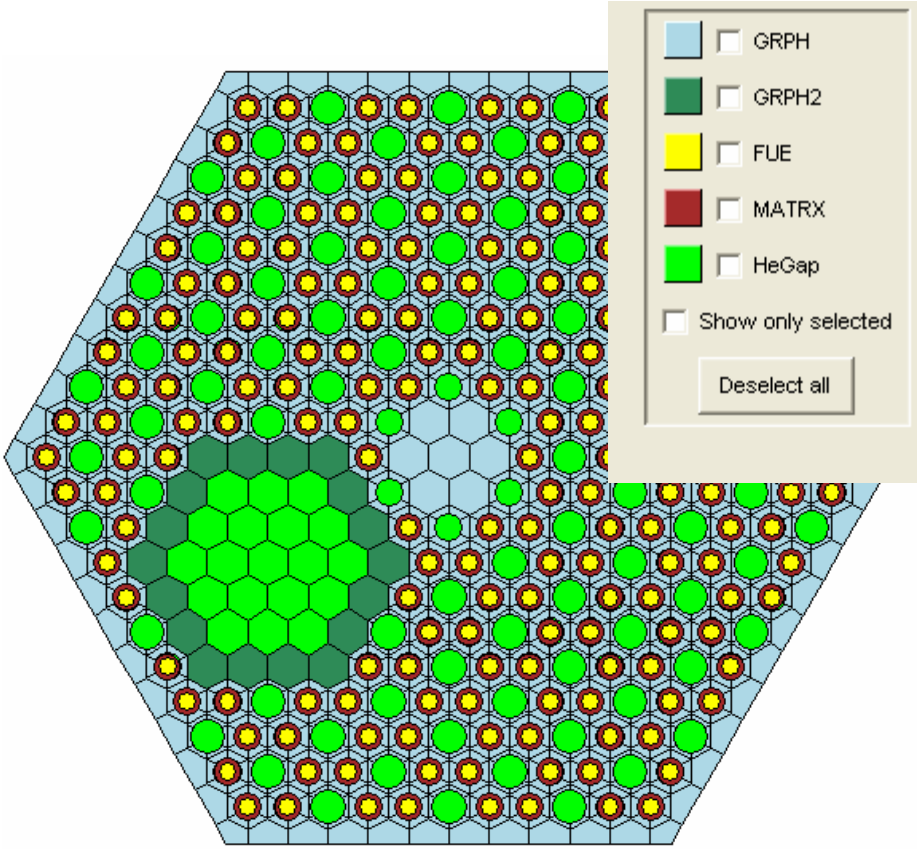

Figure 30. VHTR Fuel Block with Control Rod Hole.

The RPT approach requires equivalencing to the MCNP results. This was done for a representative fuel cell at the 300 K temperature state. In general, the new DeCART capability gives accurate assembly results for all temperature states and is quite adequate for modeling the prismatic VHTR assembly. Additional verification of assembly and core solutions is planned.

Detailed discussion on this effort will be included in the I-NERI project report due at the end of FY 2006.

4.2 UNIC Code Development

Background

The development of the whole-core neutronic code capability, the UNIC code, which can handle directly the spatial heterogeneity is ongoing at ANL. The UNIC code will use a one-stage spatial heterogeneous approach for solving the neutron transport equation, employing a large

number of neutron energy groups. The intent under this VHTR/NGNP project is to ensure that the development of the UNIC capability incorporates features that would allow its use for prismatic VHTR core analysis (with hexagonal geometry, treatment of particulate fuel, etc).

UNIC Code Status

The UNIC code is planned to compete directly with Monte Carlo stochastic based codes by using a general geometry description and a very large number of energy groups (of the order of 10,000) to eliminate spatial approximations, eliminate the lattice cross section generation step, and account accurately for energy and space resonance self-shielding effects. The intent is to provide a capability that could be used for analysis of advanced nuclear reactor designs, including fast reactor (sodium- and gas-cooled) and thermal reactor (light-water- and gas-cooled) systems.

Two methods are currently under development for the UNIC code. The first method (PnFE) is based upon the even-parity (second-order) form of the Boltzmann transport equation using the following discretization of the space-angle-energy phase space as a base method:

- multigroup energy discretization,
- three-dimensional curvilinear finite elements in space, including curvilinear elements,
- spherical harmonics expansions in angle.

The second is a Method of Characteristics (MOC) approach based upon the first-order integral transport equation. Coupling of the solution methods is ensured by continuity on boundaries of decomposed domains.

At present, the PnFE code uses a Conjugate Gradient (CG) method with automatic preconditioning to solve the within group linear system of equations. The PETSc (the Portable, Extensible Toolkit for Scientific computation) library developed at the ANL Mathematics and Computation division has been adapted for massively parallel solution of the multigroup problem. Homogeneous (power iteration) and external source problems are the current focus.

The code would be developed to run on advanced computer infrastructure employing hundreds of thousand processors.

The current accomplishments of the UNIC code development include:

- Formulation of the transport equations in second-order (even-odd parity) and integral (method of characteristics) forms for robust choices.
- Writing of the solver routine for steady state multigroup eigenvalue and/or fixed source iterations for 1-D, 2-D, and 3-D unstructured finite element mesh geometries (including capability for handling hexagonal blocks, as employed in for the prismatic VHTR).
- Initiation of work for complex geometry mesh-generation using CUBIT.
- Analysis of tracking strategy for method of characteristics solution in finite element geometry.
- Satisfactory results obtained on serial machines for standard simple benchmarks for two- and three-dimensional problems.

As illustration of the intent to ensure that the UNIC code is applicable to prismatic VHTR analysis, we first consider the mesh generator. As part of the UNIC effort, several mesh generators will be evaluated and incorporated into UNIC for effortless mesh generation. This will simplify the exchange of data for neutron transport calculations and provide detailed data for the high resolution display of results in a post-processing module. For this purpose, an evaluation of the coupling between the CUBIT code (mesh generator) and the finite elements code PnFE (finite-element, second-order form transport solver of the UNIC code) is ongoing. The first results have allowed a better understanding of its capability and at the same time provided indications of potential problems to be tackled in the future:

- The mesh generator is capable of exporting quadratic-order hexahedron that is needed for accurate treatment of curved surfaces.
- The mesh generated by CUBIT currently needs to be strictly controlled by the user such that the mesh is coarse. For transport problems, the number of elements used to

represent the structure can be coarser than those used for heat transfer and fluid-flow calculations.

- For the VHTR, a process will be developed so that the mesh is controlled by user input, saving computational time and providing an easy way to control the geometry and mesh creation process.

Figure 31 shows a prismatic VHTR assembly discretization by CUBIT that could represent a reasonable meshing for the PnFE input. The details for the fuel compact are also evident.

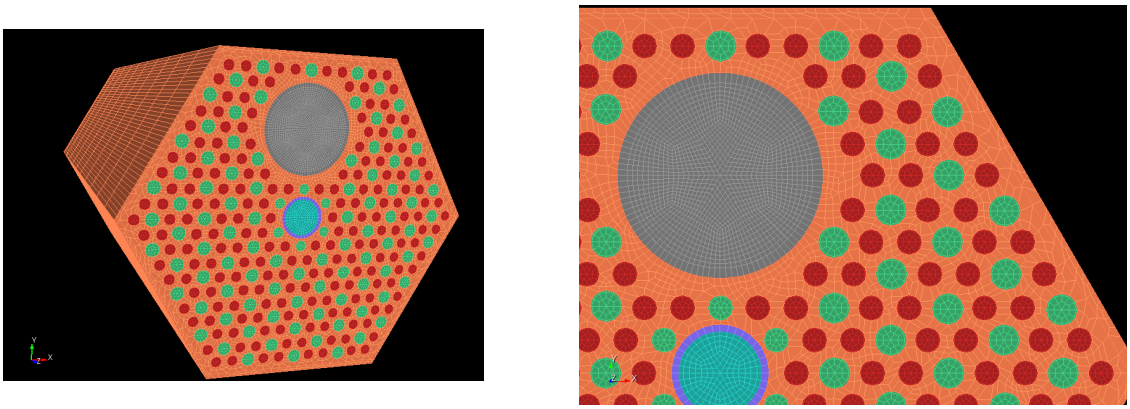

Figure 31. CUBIT Rendition of a Prismatic VHTR Fuel Block (Meshing indicated).

4.3 Final Comments

The two codes (UNIC and DeCART) that have been reviewed in Sections 4.1 and 4.2 are new capabilities that are still under development within other USDOE and international programs. The interest of this NGNP project at this time is to ensure that they provide capabilities that could be used for analysis of advanced nuclear reactor designs, including the prismatic VHTR type. This review shows that much work is still needed for these tools to be useful for routine VHTR analysis.

5.0 CONCLUSIONS

For the prismatic VHTR core design and analysis, DRAGON is selected for lattice physics calculations and REBUS-3/DIF3D for whole-core and depletion calculations. The cross section generation methodology and procedure for design and analysis of the prismatic very high temperature gas-cooled reactor (VHTR) core have been addressed for the DRAGON and REBUS-3/DIF3D code suite. Multigroup cross sections are tabulated at different burnup, and fuel and moderator temperatures so that a cross section file is able to cover the core operating range. Cross section data for points between tabulated data points are fitted simply by linear interpolation. In parallel, the functionalization of cross sections has been investigated using quadratic polynomials and linear coupling for fuel and moderator temperature changes, based on the observation that cross sections are monotonically changing with fuel or moderator temperatures. Preliminary results show that the functionalization makes it possible to cover a wide range of operating temperature conditions with only six sets of data per burnup while maintaining good accuracy and significantly reducing the size of the cross section file. In these approaches, the number of fission products is also reduced to a few nuclides (I/Xe/Pm/Sm and a lumped fission product) in order to reduce the overall computation time without sacrificing solution accuracy.

Discontinuity factors (DFs) based on nodal equivalence theory have been introduced to accurately deal with the significant change of spectrum at the interface of fuel and reflector zones as well as zones containing different types of fuel blocks (e.g., fuel elements with burnable poisons or control rods). Even though surface-dependent DFs are desirable to best account for control rods asymmetrically loaded in fuel block or reflector region, surface-independent DFs based on the simplified equivalence theory are mostly investigated and tested in this work, because a surface-dependent DF capability is not currently available for the VARIANT option of DIF3D; the VARIANT option is more accurate than the nodal option for prismatic VHTR core calculations.

With DRAGON, cross sections for fuel blocks are generated by modifying number densities of the graphite in peripheral cells because the current version of DRAGON does not allow representation of the flat boundaries of the hexagonal block. Inside peripheral cells, small

circles are configured with the same graphite material to approximate surface average fluxes without modifying the code significantly. These surface average fluxes are used to estimate DFs for the fuel block.

For reflector cross sections, a one-dimensional fuel-reflector slab model has been developed to simulate the fuel-reflector interaction of the actual core. Results indicate that the solution accuracy is improved by introducing discontinuity factors. The group sensitivity study shows that fuel block cross sections generated from the single fuel block configuration would be good enough without significant loss of accuracy if the number of energy groups is seven or higher. It is, however, noted that the accuracy can change depending on the choice of energy boundaries.

For control rod cross sections in the reflector region, two options have been explored. Option A utilizes the same one-dimensional fuel-reflector model as used for generation of plain reflector cross sections, adding a slab-type control rod in the reflector region. The location of a control rod is determined iteratively by comparing DRAGON/DIF3D results to MCNP results for a 2-D seven-block model. Two-dimensional core results show that control rod worths can be estimated reasonably, but power errors are relatively large because the power tilt due to asymmetric loading of control rods is ignored. Option B relies more on MCNP results for a 2-D seven-block model with a control rod. MCNP provides surface fluxes and currents as well as region-wise cross sections which are used for cross section generation in DRAGON and surface-dependent DF calculation in a trapezoid-based FDM code. Although this option has the potential to properly take into account both control rod worth and power tilt, it does not currently give good results for core reactivity due to the uncertainty of the MCNP results (statistical solution) and the limited use of surface-dependent DF in DIF3D.

The control rod in fuel block has been modeled with DRAGON using a two-step procedure in which homogenized cross sections are first calculated with the SYBILT option to deal with the double heterogeneity of the fuel compact and then the fuel block is computed with the EXCELT option. Due to the geometry limitation of DRAGON, an annular type control rod has been approximated with hexagonal rings.

In order to efficiently manage the developed process and partially automate a large number of routine jobs for cross section generation, a cross section management program named X-MANAGER has been developed, which is a toolkit containing many functions programmed with UNIX shell commands. Using the toolkit, it is convenient to (1) submit multiple DRAGON jobs with different temperature conditions, (2) merge many ISOTXS files into a single ISOTAB file, (3) generate reflector cross sections by executing DRAGON and the FDM code for the 1-D fuel-reflector model, (4) create delta-macroscopic cross sections for control rods by comparing unrodded and rodded ISOTAB files, etc. The X-MANAGER will be extended in the future with more functions for an advanced level of automation.

In the future, DRAGON needs to be modified to provide models for representing the flat boundary of a fuel block so that surface fluxes can be directly edited without any approximation. This code should also be able to allow multi-block calculations. In addition, the EXCELT option needs to be extended to handle the double heterogeneity arising from the coated fuel particles, such that the two-step procedure utilizing the SYBILT and EXCELT options for control rod modeling can be simplified. As discussed in Section 2.0, all verification tests have used cross sections adjusted with DFs based on the simplified equivalence theory. This is because surface-dependent DFs cannot be used in the VARIANT option of DIF3D. Therefore, the use of surface-dependent DFs should be coded in the VARIANT option in order to accurately calculate the power distribution, especially for rodded cores.

Finally, a review of the current status of the spatially heterogeneous code capabilities (UNIC and DeCART) that are being developed under other DOE and international programs was presented. These code efforts are being leveraged by this project to ensure that they provide capabilities that could be used for analysis of advanced nuclear reactor designs, including the prismatic VHTR type. Much work is still required for these tools to be useful for routine VHTR analysis.

REFERENCES

1. R. C. Potter et al., "Gas Turbine-Modular Helium Reactor (GTMHR) Conceptual Design Description Report," GA Report 910720, Revision 1, General Atomics, July 1996.

2. P. E. MacDonald et al., "NGNP Preliminary Point Design – Results of Initial Neutronics and Thermal-Hydraulic Assessment," **INEEL/EXT-03-00870** Rev. 1, Idaho National Engineering and Environmental Laboratory, September 2003.

3. T. K. Kim, W. S. Yang, M. A. Smith, T. A. Taiwo, and H. S. Khalil, "Assessment of Monte Carlo and Deterministic Codes for Next Generation Nuclear Plant (NGNP) Core Modeling," Argonne National Laboratory Gen IV Report, April 15, 2004.

4. T. K. Kim, W. S. Yang, T. A. Taiwo, and H. S. Khalil, "Whole-Core Depletion Studies in Support of Fuel Specification for the Next Generation Nuclear Plant (NGNP) Core," Argonne National Laboratory Gen IV Report, July 30, 2004.

5. G. Marleau, et al, "A User Guide for DRAGON," Technical report **IGE-174** Rev. 4, Ecole Polytechnique de Montréal, September 1998 (1998).

6. "WIMS – A Modular Scheme for Neutronics Calculations, User's Guide for Version 8," ANSWER/WIMS(99)9, The ANSWERS Software Package, AEA Technology.

7. B. J. Toppel, "A User's Guide to the REBUS-3 Fuel Cycle Analysis Capability," **ANL-83-2**, Argonne National Laboratory (1983).

8. R. D. Lawrence, "The DIF3D Nodal Neutronics Option for Two- and Three-Dimensional Diffusion Theory Calculations in Hexagonal Geometry," **ANL-83-1**, Argonne National Laboratory (1983).

9. J. F. Briesmeister, Editor, "MCNP™ - A General Monte Carlo N-Particle Code, Version 4C," Los Alamos National Laboratory, **LA-13709-M**, March 2000.

10. G. Palmiotti, E. E. Lewis, and C. B. Carrico, "VARIANT: VARIational Anisotropic Nodal Transport for Multidimensional Cartesian and Hexagonal Geometry Calculation," **ANL-95/40**, Argonne National Laboratory (1995).

11. C. H. Lee, Z. Zhong, T. Taiwo, W. Yang, and M. Smith, "Enhancement of REBUS-3/DIF3D for Whole-Core Neutronics Analysis of Prismatic Very High Temperature Reactor (VHTR)," **ANL-GenIV-076**, September 30, 2006.

12. K. Koebke, "A New Approach to Homogenization and Group Condensing," Proc. IAEA Specialists' Mtg. Homogenization Methods in Reactor Physics, Lugano, Switzerland, **IAEA-TECDOC-231**, 303 (1978).

13. K. S. Smith, "Spatial Homogenization Methods for Light Water Reactor Analysis," Ph.D. Thesis, Massachusetts Institute of Technology (1980).

14. A. Hebert, “A Collision Probability Analysis of the Double Heterogeneity Problem,” *Nucl. Sci. Eng.*, **115**, 177 (1993).

15. W. S. Yang, P. J. Finck, and H. Khalil, "Reconstruction of Pin Power and Burnup Characteristics from Nodal Calculations in Hexagonal Geometry," *Nucl. Sci. Eng.*, **111**, 21 (1992).

16. “The Numerical Nuclear Reactor for High Fidelity Integrated Simulation of Neutronic, Thermal-Hydraulic and Thermo-Mechanical Phenomena,” Final Report of US/ROK International Nuclear Energy Research Initiative Project Number 2002-010-K, Argonne National Laboratory, Korea Atomic Energy Research Institute, Purdue University, and Seoul National University, March 2005.

17. Y. H. Kim and et al., “Reactivity-Equivalent Physical Transformation for Elimination of Double-Heterogeneous Fuels,” *Trans. Am. Nucl. Soc.*, **93**, 959-960 (2005).

Nuclear Engineering Division
Argonne National Laboratory
9700 South Cass Avenue, Bldg. 208
Argonne, IL 60439-4842

www.anl.gov

A U.S. Department of Energy laboratory
managed by The University of Chicago